Final Scientific/Technical Report Submitted to:

NATIONAL ENERGY TECHNOLOGY LABORATORY (NETL) / DEPT. OF ENERGY (DOE)

Program Manager: Barbara Carney, Ph: 304-285-4671, barbara.carney@netl.doe.gov
(Previous Program Manager: Susan M. Maley)

DOE Award Number: DE-FE0007379TDD

Project Title:

WIRELESS MICROWAVE ACOUSTIC SENSOR SYSTEM

FOR CONDITION MONITORING IN POWER PLANT ENVIRONMENTS

PI: MAURICIO PEREIRA DA CUNHA,

Professor of Electrical & Computer Engineering

mdacunha@maine.edu, Phone number: (207) 581-2384, Fax number: (207) 581-2255

Submission Date: March 30, 2017.

DUNS Number: 186875787

RECIPIENT ORGANIZATION: The University of Maine
5717 Corbett Hall,
Orono, ME, 04469-5717

Project/Grant Period: Start date: Jan. 01, 2012 / End date: Dec. 31, 2016

Reporting Period: Start date: Jan. 01, 2012 / End date: Dec. 31, 2016

Report Frequency: FINAL REPORT

Digitally signed by Mauricio Pereira da Cunha
DN: cn=Mauricio Pereira da Cunha, o=University of Maine, ou=Dept. of Electrical and Computer Engineering, email=mdacunha@maine.edu, c=US
Date: 2017.06.08 16:45:39 -04'00'

2.) DISCLAIMER:

"This report was prepared as an account of work sponsored by an agency of the United States Government. Neither the United States Government nor any agency thereof, nor any of their employees, makes any warranty, express or implied, or assumes any legal liability or responsibility for the accuracy, completeness, or usefulness of any information, apparatus, product, or process disclosed, or represents that its use would not infringe privately owned rights. Reference herein to any specific commercial product, process, or service by trade name, trademark, manufacturer, or otherwise does not necessarily constitute or imply its endorsement, recommendation, or favoring by the United States Government or any agency thereof. The views and opinions of authors expressed herein do not necessarily state or reflect those of the United States Government or any agency thereof."

3.) ABSTRACT

This project successfully demonstrated *novel wireless microwave acoustic temperature and pressure sensors* that can be embedded into equipment and structures located in fossil fuel power plant environments to monitor the condition of components such as steam headers, re-heat lines, water walls, burner tubes, and power turbines. The wireless microwave acoustic sensor technology researched and developed through a collaborative partnership between the University of Maine and Environetix Technologies Corporation can provide a revolutionary impact in the power industry since it is anticipated that the wireless sensors will deliver reliable real-time sensing information in harsh power plant conditions that involve temperatures up to 1100^{o}C and pressures up to 750 psi. The work involved the research and development of novel high temperature harsh environment thin film electrodes, piezoelectric smart microwave acoustic sensing elements, sensor encapsulation materials that were engineered to function over long times up to 1100^{o}C, and a radio-frequency (RF) wireless interrogation electronics unit that are located both inside and outside the high temperature harsh environment. The UMaine / Environetix team have interacted with diverse power plant facilities, and identified as a testbed a local power generation facility, which burns municipal solid waste (MSW), the Penobscot Energy Recovery Company (PERC), Orrington, Maine. In this facility Environetix / UMaine successfully implemented and tested multiple wireless temperature sensor systems within the harsh-environment of the economizer chamber and at the boiler tubes, transferring the developed technology to the power plant environment to perform real-time sensor monitoring experiments under typical operating conditions, as initially targeted in the project. The wireless microwave acoustic sensor technology developed under this project for power plant applications offers several significant advantages including wireless, battery-free, maintenance-free operation, and operation in the harsh-environment of power plant equipment up to about 1100 ^{o}C. Their small size and configuration allows flexible sensor placement and embedding of multiple sensor arrays into a variety of components within power systems that can be interrogated by a single RF unit. The outcomes of this project and technological transfer respond to a DOE analysis need, which indicated that if one percent efficiency in coal burning is achieved, an additional 2 gigawatt-hours of energy per year is generated and the resulting coal cost savings is $300 million per year, also accompanied by a reduction of more than 10 million metric tons of CO_2 per year emitted into the atmosphere. Therefore, the developed harsh environment wireless microwave acoustic sensor technology and the technological transfer achievements that resulted from the execution of this project have significant impact for power plant equipment and systems and are well-positioned to contribute to the cost reduction in power generation, the increase in power plant efficiency, the improvement in maintenance, the reduction in down-time, and the decrease in environmental pollution. The technology is also in a position to be extended to address other types of high-temperature harsh-environment power plant and energy sector sensing needs.

4.) TABLE OF CONTENTS

5.) EXECUTIVE SUMMARY

The overall goals of this project were to develop and demonstrate the performance of wireless microwave acoustic temperature and strain sensors that are embedded in equipment and structures located in fossil fuel power plant environments to monitor the condition of components, such as steam headers, re-heat lines, water walls, burner tubes, and power turbines. The project, originally planned as a three-year project, was extended to an additional two years, which allowed transitioning of the developed technology to practical applications, in particular through the installation and testing of wireless surface acoustic wave (SAW) sensor arrays in the economizer and boiler tubes of the Penobscot Energy Recovery Company (PERC), Orrington, Maine. This power generation facility burns municipal solid waste (MSW) and was found to be an appropriate testbed to evaluate the wireless SAW sensor technology both due to the nature of the power plant harsh environment condition and the proximity to the Laboratory for Surface Science and Technology (LASST) at the University of Maine (UMaine) and Environetix Technologies Corporation in Orono, ME, who partnered in the execution of this project.

The harsh-environment technology developed consists of small, battery-free SAW sensors and integrated antennas, which are embedded directly into power generation structures and components, and interrogated wirelessly with a stand-alone radio frequency (RF) electronics unit located outside the high-temperature harsh environment. To realize this wireless sensor system, researchers from LASST at the UMaine and personnel from Environetix performed research and development (R&D) activities that focused on highly reliable and stable sensor prototypes comprised of novel high-temperature harsh-environment piezoelectric smart sensing elements, consisting of electrode and sensor encapsulation materials capable of operating above 1000ºC and pressures up to 750 psi.

The work was built on patented UMaine wireless microwave acoustic sensor technology that has been demonstrated by the UMaine / Environetix team to operate at 800ºC for 5½ months in laboratory furnaces and up to 700ºC on rotating parts in scaled turbine engines.

Under specific accomplished objectives for the current project one can list: (1) Advancement of novel thin film nanocomposite electrodes for wireless SAW sensors to achieve stable and reliable operation above 1000ºC and towards 1200ºC; (2) Development of sensor interrogation methods and sensor encapsulation materials and techniques for embedding sensor arrays into power plant components; and (3) Demonstration of the viability of prototype sensor arrays and interrogation systems through laboratory furnace and power plant field testing.

Under the advancement of novel thin film nanocomposite electrodes for wireless SAW sensors to achieve stable and reliable operation at high-temperature harsh-environment conditions significant progress was made. The previous technology developed by UMaine, namely a $Pt/Rh/ZrO_2$ film showed to be inappropriate for long-term operation above 900°C. Significant part of this project was devoted to the identification and development of new electrodes capable of withstanding higher temperatures. A wide range of prospective multi-layered and co-deposited Pt alloy electrode materials have been screened including Pt or PtRh combined with alloying elements Co, Ni, Cr, Rh, Ta, Ti, Nb, Al, Sn or oxides HfO_2, ZrO_2, Nb_2O_3, Y_2O_3, RuO_2, CeO_2, NiO, CoO, MnO_2. Successful electrode materials that resulted from this research are based on several thin film materials and structures including a PtNi|PtZr alloy; a Pt/Al_2O_3 film, and a

PtRh/HfO_2 film. These electrode materials, first investigated through blanket wafers, have been used to fabricate photolithographically patterned SAW devices which have been successfully operated at 1000°C and above.

As part of the encapsulation effort and electrode improvement to achieve stable operation in high-temperature harsh-environment, both interfacial layers and capping layers were investigated under this work. An atomic layer deposition (ALD) techniques was used to deposit a 50nm thick Al_2O_3 layer on top of the langasite piezoelectric substrate (interfacial layer) and also on top of the entire device (capping layer). The capping layers delayed the interaction of the electrode material with the substrate, thus extending in temperature the performance of the thin film electrode. At temperatures beyond 1000°C, electrode stability is challenged by the strong thermodynamic driving forces that cause film agglomeration and interdiffusion phenomena. The ALD Al_2O_3 capping layer was identified to delay the agglomeration process, thus extending in temperature and time the operation and performance of the Pt-based thin film electrodes. In addition to the thin film agglomeration, at temperatures approaching 1000°C the 25μm (1mil) Pt bonding wire contact to the sensor undergo major morphological changes, thus accelerating the electrical discontinuity around the bonding area. Since the ALD Al_2O_3 capping layer is an insulator, bonding to the Pt wire becomes problematic, and thus a capacitive coupling technique was established to electrically access the device across the insulating capping layer and provide reliable operation at temperatures at or beyond 1000°C.

Wired and wireless testing of packaged prototype SAW sensors have been performed twice at the National Energy Technology Laboratory (NETL) Aerothermal facility, Morgantown, WV, exposing several sensors and packaging fixtures to 1100°C and pressures up to 50psi. The successful tests performed at the NETL Aerothermal facility were fundamental to the development and further technology transition to the PERC power plant previously mentioned. In order to be installed in power plant environments diverse encapsulation methods have been developed using alumina, macor, and Inconel materials as basic insulators and conductors for connection, antenna, and packaging cases.

This work resulted in 24 publications, was disseminated through 26 national and international conferences to diverse audiences, which include materials science conferences, microwave acoustic symposia, DOE conferences, web seminars, and local presentations. In addition to UMaine and Environetix, the effort involved multiple institutions at levels which included collaboration, consultation, multiple visits, application analysis, web presentations and conferences, namely: PERC, NETL/DOE, GE Energy, Siemens Energy, Alstom, Brayton Energy, Duke Energy, Electric Power Research Institute, Exxon. Throughout the period of execution, the PI and Co-PI trained fourteen senior and junior researchers and engineers, three graduate students, and eleven undergraduate students. Performance of thin film electrodes and other layers affect the broader areas of microwave acoustics and high temperature thin film materials, and significantly establish new metrics of performance for high-temperature harsh-environment wireless SAW sensors. The positive results and achievements of this project confirmed the maturity of the wireless SAW sensor technology and demonstrated the technology operating in a real power plant environment. The maturity of the technology will continue to be realized by future research and development projects that will extend the wireless SAW sensor technology to other types of sensing needs in high-temperature harsh-environment power plant conditions.

6.) REPORT DETAILS

6.1 EXPERIMENTAL METHODS

This section provides a comprehensive summary of the experimental methods employed on the various phases of this project. For further details on the project implemented methods, the reader is invited to check the published material, listed in Section 8, *References*.

6.1.1 Thin-Film Investigation & Fabrication for High-temperature Operation

In order to increase the operational temperature of the high-temperature SAW sensors one of the limitations at the beginning of the project was the thin-film electrode utilized for the device interdigital transducers (IDTs) and reflector structures. The IDTs are responsible to transducing the electric signal into the electro-mechanical wave that propagates in the SAW sensor.

The thin-film electrode degrades with temperature by agglomerating into islands of conducting material, which in the case of the films studied in this work were platinum-based (Pt) alloys. The agglomeration culminates in the total isolation of these islands, in which situation the film is no longer a conductor. The scanning electron microscopy (SEM) shown below illustrates the issue.

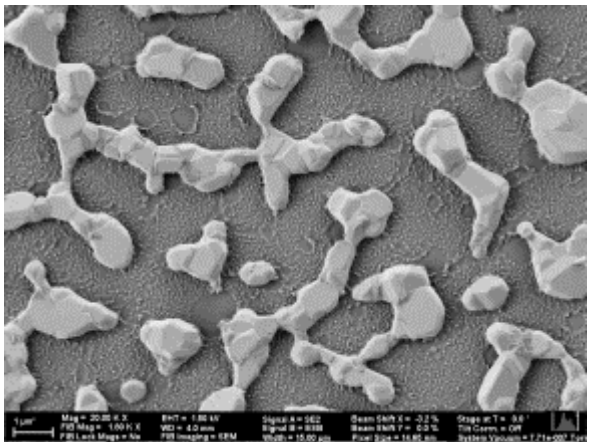

Figure 1: SEM images of Zr|PtRh alloy film after heating for 4 hrs in air at 1000°C.

Therefore one of the first tasks in the project was to characterize the short and long term degradation of the existing thin-film electrode, and then attempt to increase the temperature of performance of the electrode thin film towards 1000°C and if possible beyond that value. The piezoelectric substrate used in the project for the SAW generation is langasite (LGS, $La_3Ga_5SiO_{14}$), which has a melting point of 1476°C. This material has shown good mechanical stability tested up to 1300°C, with no change in phase or significant crystal degradation, and no identifiable degradation of its piezoelectric properties once returned to room temperature.

Procedures for Film Deposition and Characterization

Platinum-based films were grown on pieces of 0.5 mm thick LGS crystals at room temperature in a vacuum chamber with typical base pressures in the 10^{-8} to 10^{-9} torr range. Materials were deposited by electron beam evaporation of ≥ 99.9% purity metal source materials in vacuum or grade 5.0 oxygen environments of approximately $2x10^{-5}$ torr, depending on desired film composition. Platinum-rhodium composition films were deposited by evaporation of Pt10(wt%)Rh alloy, whereas all other materials were evaporated from a single element charge. Both Zr and Hf films of 7.5 nm thickness were used as adhesion layers. Following deposition, the samples were diced to dimensions of 3 mm x 7 mm for furnace heating and resistivity measurements. Figure 2 shows the thin film vacuum chamber schematics and a picture of the equipment. Without breaking the vacuum, this equipment allows allows for x-ray photoelectron spectroscopy (XPS) to be performed.

Accurate monitoring of the evaporant rate from the two electron beam deposition sources is critical for obtaining desired film compositions and thicknesses. The rates for each source were monitored independently by two quartz crystal rate monitors (QCMs). For the QCM controller to calculate film deposition rate/thickness from the oscillator frequency shift, three parameters are entered: tooling factor (ratio between QCM/sample flux), film density, and Z-factor (related to the density and shear modulus of quartz/film material). Tooling factors were determined for the electron beam evaporator QCMs by depositing individual films of 10 to 20 nm while comparing the thicknesses using identical material parameters for a QCM positioned at the sample plane and one placed at the evaporator monitoring position. Film densities for each material were determined by using the measured tooling factor and a tabulated value for density, by depositing films ≥ 50 nm on polished fused silica substrates with a shadow mask to define a 0.25 mm stripe, and by measuring the height of the stripe with a stylus profilometer. The actual film density was calculating by using the ratio of the QCM and profilometer measured thicknesses.

The Z-ratio contributes only a small correction and tabulated values will be used for all depositions. For co-deposited materials, the composition and thickness of the film was established by manual control of the electron beam evaporator power based on rate measurements using each respective QCM with the appropriate calibrated density value. Profilometry following deposition was used to obtain actual film thickness.

In addition to the XPS technique for film characterization, other equipment present at the Laboratory for Surface Science and Technology, the University of Maine, and used to characterize the thin film electrodes in this work were: x-ray diffraction (XRD), atomic force microscopy (AFM) and high resolution scanning electron microscopy (SEM).

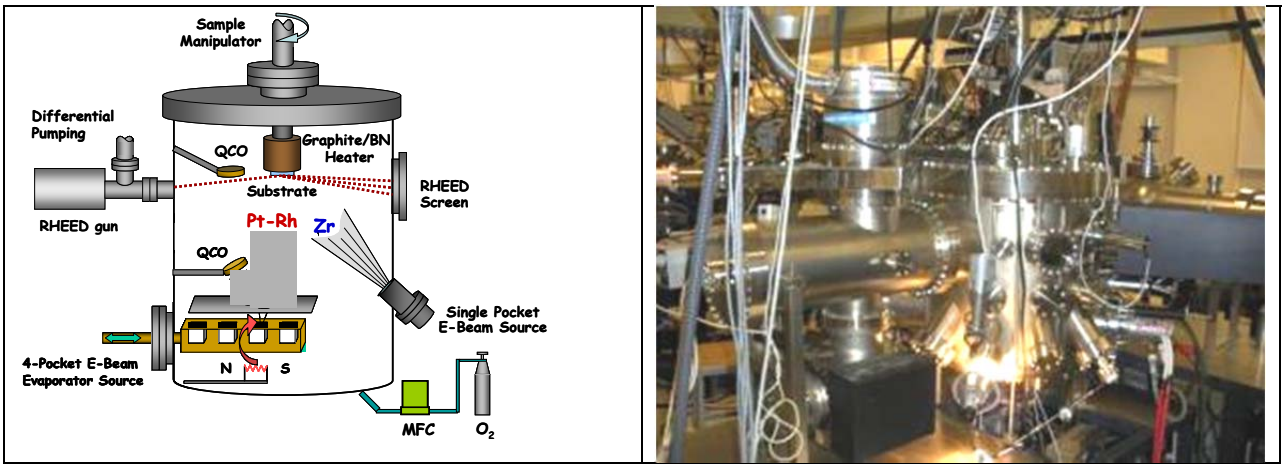

Figure 2: Nanocomposite Electrode Chamber: details of the deposition system (left) and actual deposition and characterization chamber.

Thin-film Characterization Technique

A method to screen and evaluate the resilience and performance of thin-film electrode materials at temperatures up to 1200°C was developed. A tube furnace (Figure 3) was employed to heat different samples at different temperature at the same time, a task that could not be achieved with a box furnace. The tube furnace has a temperature gradient that has been mapped out using a custom built S-type thermocouple probe (see Figure 3). A custom sample holder fixture (Figure 4) has also been assembled that will precisely place the samples at locations in the furnace corresponding to 800, 900, 1000, 1050, 1100, 1150, and 1200°C. The sample size and furnace uniformity are such that up to 6 different samples can be placed at each temperature point with an estimated temperature uniformity of better than ±10°C across the samples (Figure 5).

In prior tests at UMaine up to 1000°C, real-time 4-wire resistance measurements were made during furnace heating of the samples. To make such measurements, contact to the films was made by parallel gap welding 25 µm diameter Pt wires to blanket-deposited films. Parallel gap welding causes localized melting and leads to chemical changes at the interface between the bond wires and film. Furthermore, at the extreme temperatures under consideration, solid state diffusion kinetics can be rapid and can lead to bond deterioration. Although a 4-wire measurement eliminates the resistance of the leads, the interface resistance cannot be eliminated and will be measured in series with the film resistance. To avoid possible artifacts due to reactions at the bond wire / film interface, it was decided that initial screening of new materials at temperatures up to 1200°C will be performed without the use of wire bonding. Samples will be heated to a range of temperatures, removed from the furnace, and 4-point resistivity measurements will be made at room temperature to evaluate the effect of heating on the electrical properties.

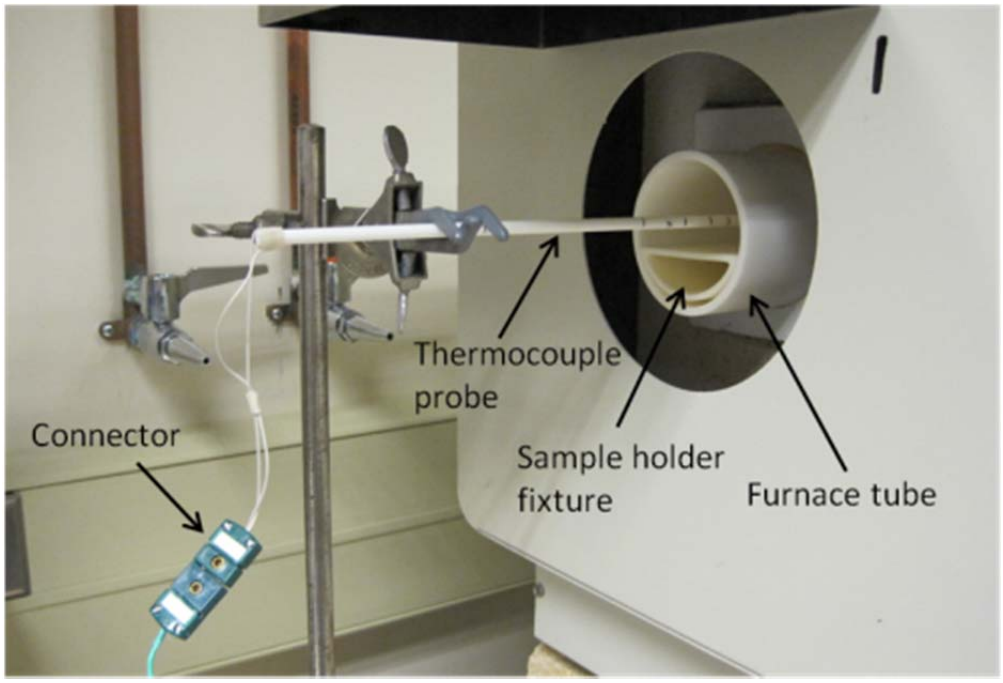

Figure 3: Custom thermocouple probe inserted in tube furnace for temperature profile measurement

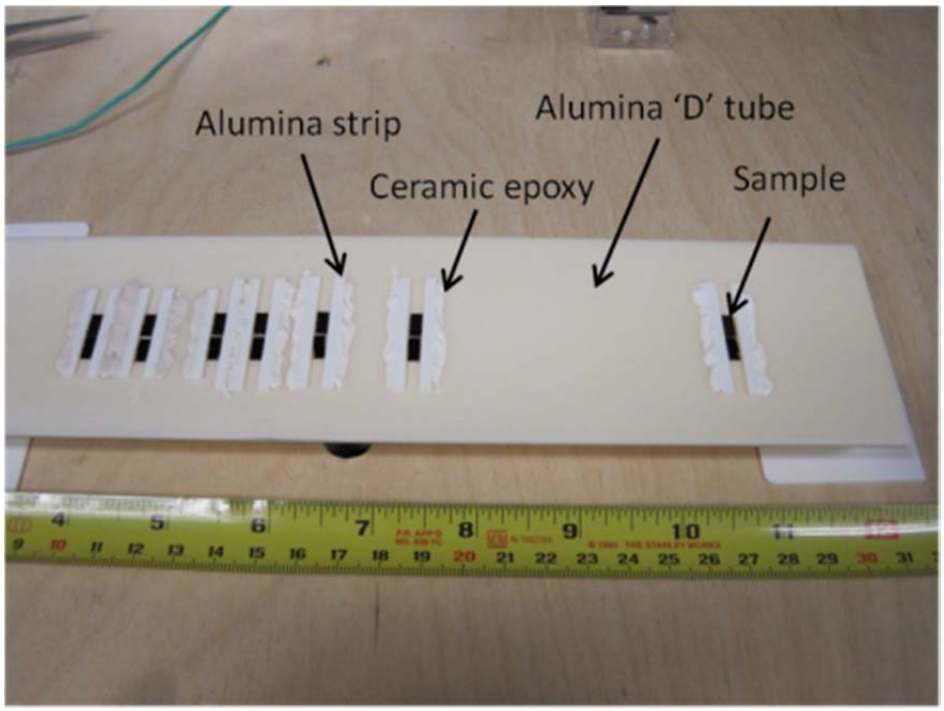

Figure 4: Custom built tube furnace sample holder. Alumina strips were attached to an alumina tube with a 'D' shaped cross section to create 3.5 mm slots for 3 mm samples.

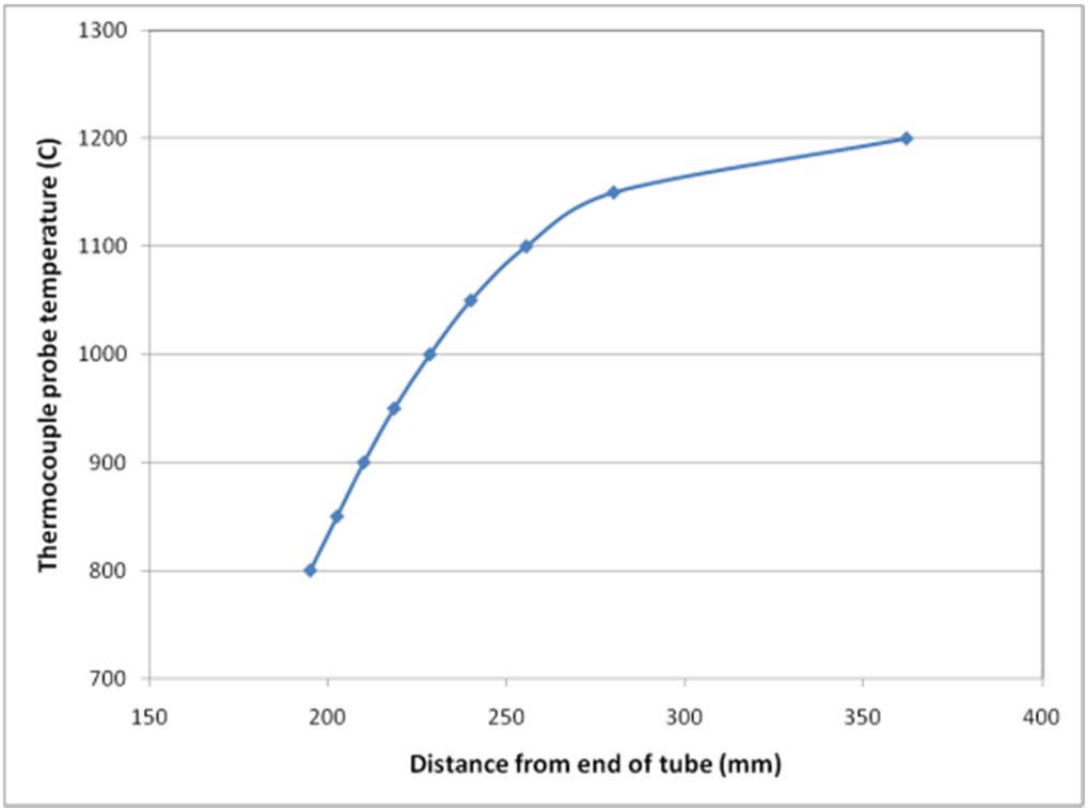

Figure 5: Temperature map of tube furnace fixture - center of furnace held at 1200ºC

6.1.2 High-Temperature SAW Sensor Fabrication and Characterization for High-Temperature Harsh-Environment Operation

SAW Device Fabrication

The SAW devices were fabricated at the clean room facilities present at the Laboratory for Surface Science and Technology at the University of Maine, employing standard photolithographic lift-off techniques. Inside the clean room facilities the optically polished LGS wafer is further cleaned to remove any surface contaminant or particle which could compromise the definition of the micrometer size SAW device features. After cleaning, regular photolithographic patterning was used to transfer the devices patterns from a externally fabricated mask onto the surface of the LGS. Computer aided design tools available at the Microwave Acoustic Laboratory (MAL) at UMaine were used to define the pattern used to generate the photolithographic mask.

The wafer was transferred to the electrode deposition chambers mentioned in the previous Section 6.1.1 for the desired electrode metallization deposition, and after that returned to the

clean room to finalize the lift-off procedure, removing the metal deposited on top of the photoresist, and thus defining the targeted SAW device pattern.

Most of the devices fabricated under this project operated at one of these bandwidths: (i) 175 to 195 MHz; or (ii) 280 to 330 MHz. The first have smallest features around 3.5μm, whereas the second group had features around 2μm. Different masks were fabricated for devices operating in these frequency ranges. The selection of these operating frequency bands were based on the dimension which allowed reliable fabrication at UMaine facilities and reliable operation at high-temperature.

Typical 2 μm wide electrode devices had an acoustic aperture of 51 wavelengths, a nominal mark-to-space ration of 1:1, IDTs 40.5 wavelengths long, and two open-circuit reflectors with 400 electrodes. The 2 μm wide electrodes devices were fabricated along LGS Euler angles (0°, 138.5°, 20.5°), resulting in a nominal center frequency of 330 MHz. The lower frequency group of devices had an acoustic aperture of typically 31 wavelengths, a nominal mark-to-space ratio of 1:1, IDTs 80.5 wavelengths long, and two open-circuit reflectors with 500 electrodes. For the lower frequency devices, the electrodes were 3.5 μm wide and the device was fabricated along LGS Euler angles (0°, 138.5°, 26.7°), resulting in a nominal center frequency of 194 MHz.

Other Thin-film Techniques Employed in the SAW Device Fabrication

Adhesion Layer / Multilayered

A 10 nm Zr adhesion layer was first deposited on the LGS substrates by electron beam evaporation in a custom ultra-high vacuum deposition chamber (10^{-9} Torr). The thin film adhesion layer is essential to promote the adhesion of the metallic layer to the substrate. Failure to deposit this adhesion layer caused the delamination of the metallic layer with poor or no piezoelectric transduction.

The electrodes were deposited by electron beam evaporation of alternating layers of Pt-Rh and Hf in a 10^{-5} Torr O_2 partial pressure, or a combination of co-deposited metals depending on the type of electrode used. In case of the layered electrodes, and typically eight layers were used, with a nominal total thickness of 120 and 190 nm for the 330 and 194 MHz devices, respectively.

Annealing and Temperature Cycling

Devices were normally annealed at 850°C for 4 hrs to increase the conductivity of the electrode layer by densification and precipitate formation. The annealing time and temperature varied according to the type of film deposited. If no electrode annealing is executed, the electrodes present a very high-resistivity, resulting in very poor transduction and SAW device performance.

In order to provide sensor stabilization, another technique used was cycling the temperature between low temperatures (100°C, or 200°C, or 300°C) and high temperatures (700°C, or 850°C, or 1000°C).

SAW Device Characterization

The SAW resonator sensor were characterized using on wafer measurements performed at room temperature or mounting & packaging methods for furnace testing. The on-wafer tests were performed with the aid of a Cascade™ Microtech probe station (Cascade Technologies, Inc., Beaverton, OR.) shown in Figure 6.

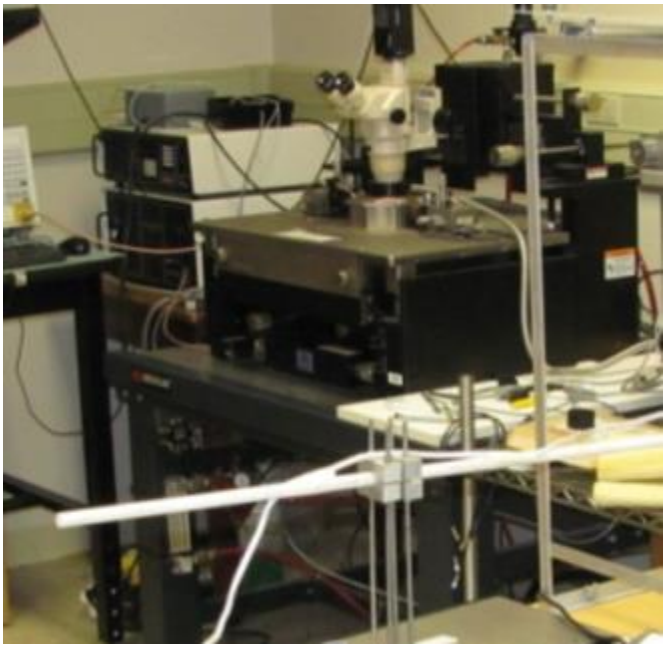

Figure 6: Cascade™ Microtech probe station utilized for on-wafer SAW sensor characterization at room temperature

When high temperature box furnace testing was performed, a Unitek parallel gap welder (Miyachi Unitek, Monrovia, CA) with 1 and 4 mil Pt wire was employed for the device packaging. The reported high temperature tests were performed at atmospheric pressure in laboratory air using Thermolyne box-furnaces (Thermolyne, Dubuque, IA), as shown in Figure 7. The SAW device responses were monitored with an Agilent 8753ES network analyzer (Agilent Technologies, Santa Clara, CA) or other equivalent bench or portable vector network analyzer available in the MAL/UMaine.

Also shown in Figure 7 is a typical high temperature fixture packaging: the SAW is mounted on Inconel plates and held in place using 3 or 4 mil Pt wires, while the electronic access to the

device normally uses 1 mil Pt wires due to the thin film thickness, and connects the sensors to high-temperature Inconel coaxial cables (Figure 7, right).

Figure 7: Box-furnace testing and typical fixture: (Left) SAW devices located inside the box oven; and (Right) LGS SAW resonator devices packaged on an Inconel plate.

6.1.3 Thin-Film Improvements for High-temperature SAW Sensor Operation

Motivation

For stable sensor operation with long term survivability and low drift under high-temperature harsh-environment conditions, it is very critical to have a stable ultra-thin (≈200 nm) electrode material that exhibits minimal agglomeration, electromigration, and oxidation. In addition, the electrode material should be a reasonably good conductor for appropriate SAW excitation and detection, as discussed in Section 6.1.1. Platinum, the best noble metal for high temperature thin film sensor electrodes, agglomerates at ≈700°C, forming metal islands that yield an electrical discontinuity. SAW resonators fabricated at UMaine with Pt-Rh/ZrO_2 electrodes prior to this project have been shown to exhibit stable sensor behavior for more than 5½ months at 800°C. However at temperature approaching 1000°C and beyond, this electrode film failed and new materials and technics have to be introduced to establish stable operation of the LGS SAW high temperature sensors.

New Electrode Materials

In addition to the Pt-Rh/ZrO_2 IDT electrodes previously mentioned in this report, a series of alternative thin film electrode materials with potential for operating at high-temperature have been investigated using both co-deposited and multilayered deposition techniques. The thin film electrode materials that have been investigated include: PtCo, Pt-Rh/CoO, PtNi, Pt-RhNiO, PtCr,

Pt-Al, Pt-Al/Pt/ZrO_2, Pt-Al/Pt/Nb, Pt-Al/Pt/Cr, Pt-Al/Pt/ZrO_2, PtAl_2O_3, Pt-Rh/HfO_2, among others. The research and development of these films allowed the extension of the operational temperature of the SAW sensors from 800°C to above 1100°C, as presented in Section 6.2 of this report.

Description of New Methods & Techniques for High-Temperature SAW Fabrication

In addition to the new electrode materials, new techniques for the film fabrication were required to increase the operational temperature of the SAW sensor devices from 800°C to above 1100°C. These techniques are labeled here as: pinning materials, interfacial layer, and capping layer.

Pinning Materials

The function of the pinning is to retard the agglomeration process which takes place with the thin-film platinum electrodes. Several pinning materials were investigated: ZrO_2, MnO_2, CeO_2, NiO, HfO_2, CoO, Al, and ZrC added to $Pt_{83}Rh_{17}$ films on sapphire substrates. In addition, four prospective oxide pinning materials: HfO_2, Y_2O_3, Nb_2O_3, and RuO_2 were tested on langasite substrates and compared to ZrO_2, Zr, and no pinning phases. Most of the films were grown in a $2.7x10^{-3}$ Pa background of O_2 to create oxide pinning phases during the deposition; subsequent air annealing caused the pinning metal components in all the films to reach their maximal valence oxide state.

While the pinning materials serve the important function of increasing the SAW sensor operational temperature, one of the drawbacks is that their oxide nature also diminishes the film conductivity.

Interfacial Layer

Interactions between the electrode film and the LGS substrate once the sensor is exposed to temperature approaching 1000°C favor the thin-film agglomeration process. Thin film electrodes deposited on sapphire substrate showed that the agglomeration was retarded and/or occurred at higher temperatures when the electrode film was deposited on top of sapphire as opposed to LGS. For this reason, an Al_2O_3 surface passivation layer, labeled in this work as interfacial layer, deposited by atomic layer deposition (ALD) was employed. The aim of the interfacial layer is to reduce electrode deterioration by minimizing interdiffusion and chemical reactivity with the LGS substrate. Figure 8 depicts a cross section of the SAW sensor at the location of a contact bus-bar, showing the ALD interfacial layer, among other structures used in the electrode fabrication and discussed next in this section.

Capping Layer

In previous work performed by the UMaine, a SiAlON capping layer over Pt-Rh/ZrO_2 SAW sensor IDTs was used to delay film agglomeration up to 900°C. In this project, an Al_2O_3 capping layer deposited by ALD was employed to perform the same passivation function for operation beyond the 900°. The capping layer is important to retard the thin-film agglomeration process and also to reduce the formation of whiskers, as mentioned further on in this report. The capping layer is also depicted in Figure 8.

Capacitive Coupling

Covering the entire surface of the LGS SAW sensor with the Al_2O_3 ALD capping layer brought the issue of how to electrically access the bus-bars or bonding pads of the IDT for electro-acoustic transduction. In addition, the connection to the SAW sensors through Pt bonding wires is limited to temperatures below 1000°C due to the deterioration of the thin-film in the vicinity of the bonding location at those temperatures, mostly due to the agglomeration effect.

To overcome these issues, capacitive coupling was introduced in this work. The idea is that the deposition of a an electrode film on top of the Al_2O_3 ALD forms a capacitor, which allows for proper alternated current (AC) connection to the SAW device at the desired operating frequency. The film deposited on top of the Al_2O_3 ALD layer was fabricated using Pt thick paste on top of the Pt thin film and Zr adhesion layers. The use of the thick film paste allowed for easier and more reliable wire bonding and high temperature contact performance. The structure is depicted in Figure 8.

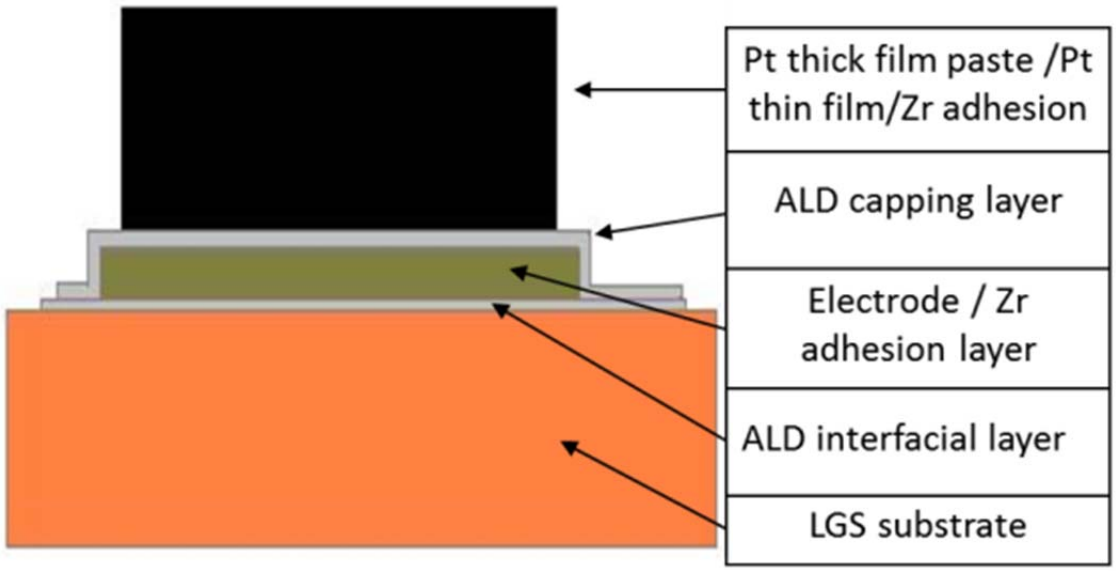

Figure 8: Cross section of an LGS high temperature SAW resonator sensor showing the different layers used during IDT and electrode fabrication.

6.1.4 In-house Developed Wireless Temperature-Profile Furnace

Motivation & Description

The existence of a testbed for wireless interrogation of SAW sensors at a high temperature is useful for the development of the sensor and the wireless interrogation technique. The existing box furnaces are made of metal, which therefore works as a shield for electromagnetic signals

being sent from outside the furnace. For this reason, a high temperature furnace with insulating walls and not enclosed in a metal box and capable of operating up to 1200°C was designed and fabricated in this project. Figure 9 shows the mentioned furnace. The metallic heat shield is removable, and the SAW sensor inside the furnace can be interrogated wirelessly by and antenna outside the furnace.

Figure 9: High-temperature antenna-testing laboratory furnace

6.1.5 Methods for Testing in Power Plant Environment

Motivation & Description

One of the goals of this project was to test and validate the wireless high-temperature SAW sensor technology researched and developed in meaningful power plant environments. This goal was achieve by testing the technology in two major testbeds: the National Energy Technology Laboratory (NETL) Aerothermal Facility, Morgantown, WV; and at the Penobscot Energy Recovery Company (PERC), Orrington, ME, a power plant which burns municipal solid waste (MSW), and thus have the sensors, packaging, antenna fixtures and electronics exposed to an extremely harsh testing environment containing highly erosive and corrosive gases.

Figure 10 shows the NETL Morgantown Aerothermal Facility testbed and one of the tests performed, where SAW sensors, antennas, and packaging materials have been exposed to temperature in the in the 700°C to 1100°C range. Pressure in this chamber was also abruptly changed between atmospheric pressure, 30psi, and 60psi. Temperatures at the wall of the chamber reach up to 850°C, whereas temperature a few millimeters away from the wall reach 1100°C. Figure 11 shows the PERC power plant facility and the economizer chamber, with an

access port, which allowed tests not only in the economizer chamber, but also on the last section of the boiler tubes, as detailed later in this report.

For both the NETL Aerothermal facility tests and for the PERC power plant tests, the methodology for tests included prior tests of packaging materials endurance to the respective environments. Based on the results of these material tests the Environetix/UMaine team designed and implemented the wireless SAW sensors arrays, antennas, and respective packaging to be further tested as an integrated system.

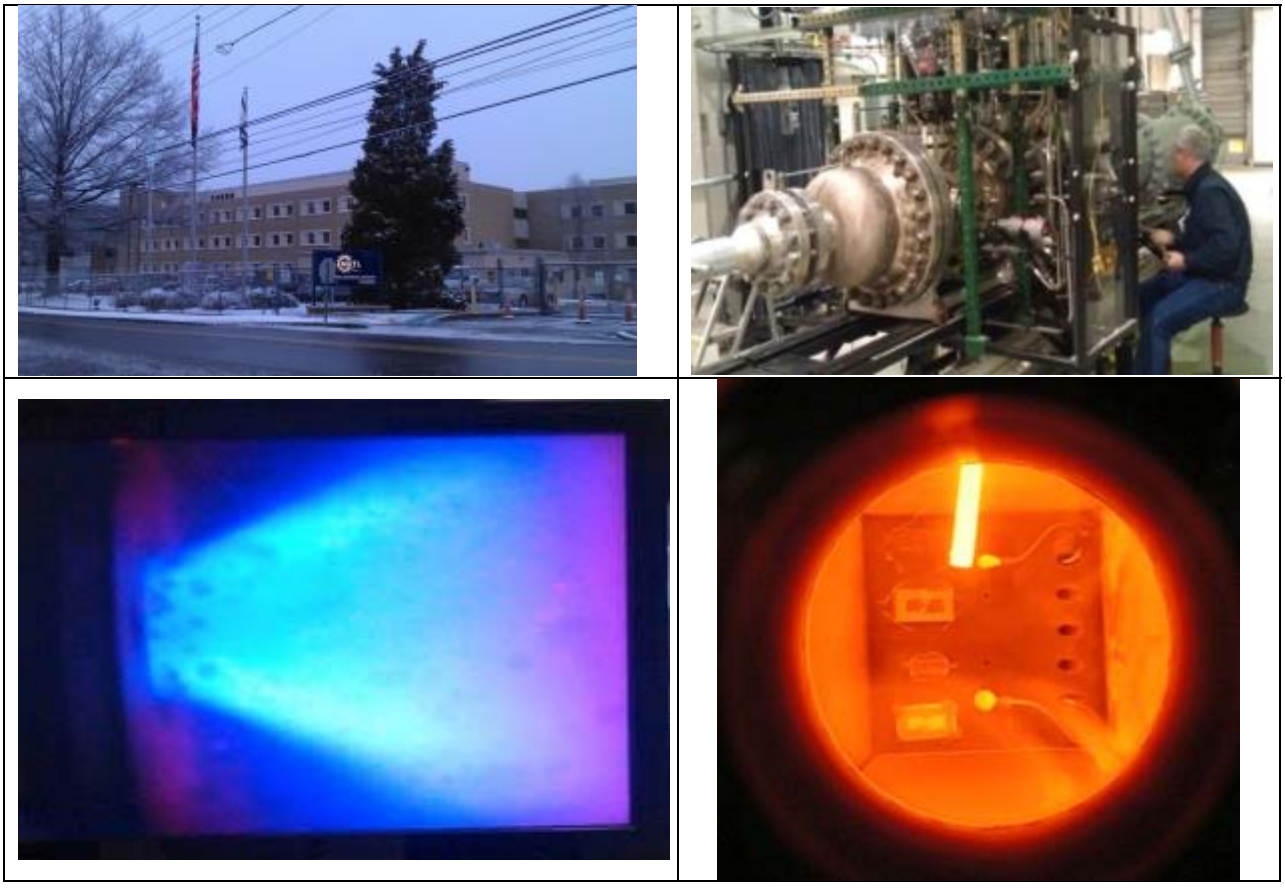

Figure 10: (Top-left) NETL Morgantown, WV facility; (Top-right) NETL Aerothermal Facility testbed; (Bottom-left) location in the vicinity of the nozzle, where the test coupon was placed; (Bottom-right) window view of the SAW sensors and packaging exposed to temperatures to temperatures in the 700°C to 1100°C range.

Figure 11: (Top-left) Penobscot Energy Recovery Company (PERC) power plant facility; (Top-right) Garbage separation in preparation for burning; (Bottom-left) Back of the boiler section and economizer region, with access port, where different wireless sensor array architectures were tested; (Bottom-right) Environetix engineer performing a wireless SAW sensor array routine monitoring.

Tests at NETL Aerothermal Facility, Morgantown, WV & Description

Figure 12 shows internal details of the Aerothermal testbed, a natural gas combustor, which photograph is shown in Figure 10. The test coupon was directly exposed to harsh-environment by being mounted in the test section of the exhaust. An inner viewport window allowed for the visual monitoring of the fixture and devices' integrity. After the first test, which allowed for the screening of the best high temperature materials and mounting, a second test verified both wired and wireless sensor packaging and performance, comparing the results to thermocouples mounted in coupon, side-by-side with the SAW sensors. For this second test, cables and wires were transitioned from the room temperature section to the hotter section of the access point, location labeled in Figure 12 as *Cooling Air Plenum*.

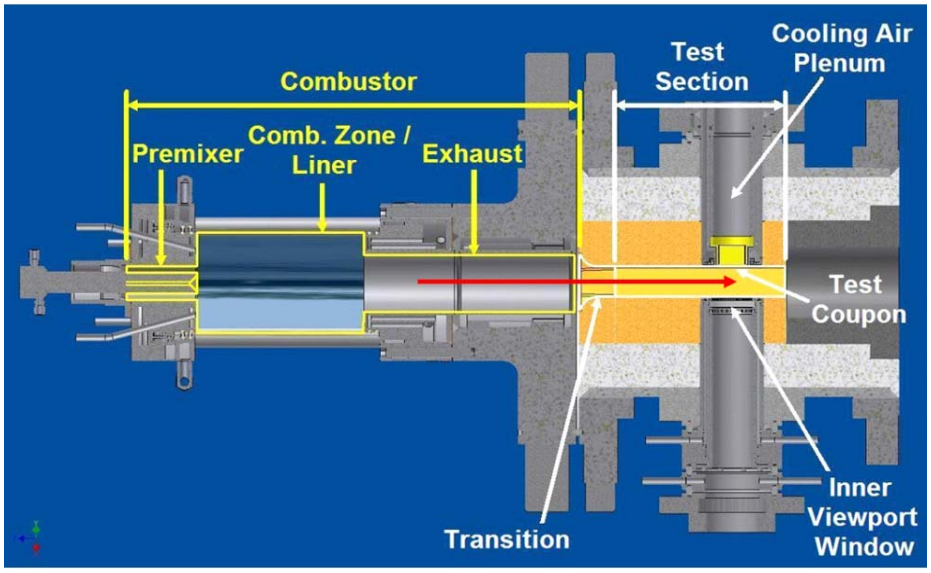

Figure 12: Schematic of the Aerothermal test fixture (photograph shown in Figure 10)

Tests at PERC Power Plan, Orrington, ME & Description

Figure 13 shows the schematic of the PERC facility testbed, a detail of the economizer access point, and a SAW sensor array panel, containing six sensors wireless interrogated by a monopole interrogating antenna, also included in the panel. The economizer was selected for the SAW sensor array placement due to the existence of an access door, which allowed sensor access and monitoring with minor disruption to the power plant activities. Also shown in **Figure 13** are the details of the sensor placement, sensor antenna, and overall packaging.

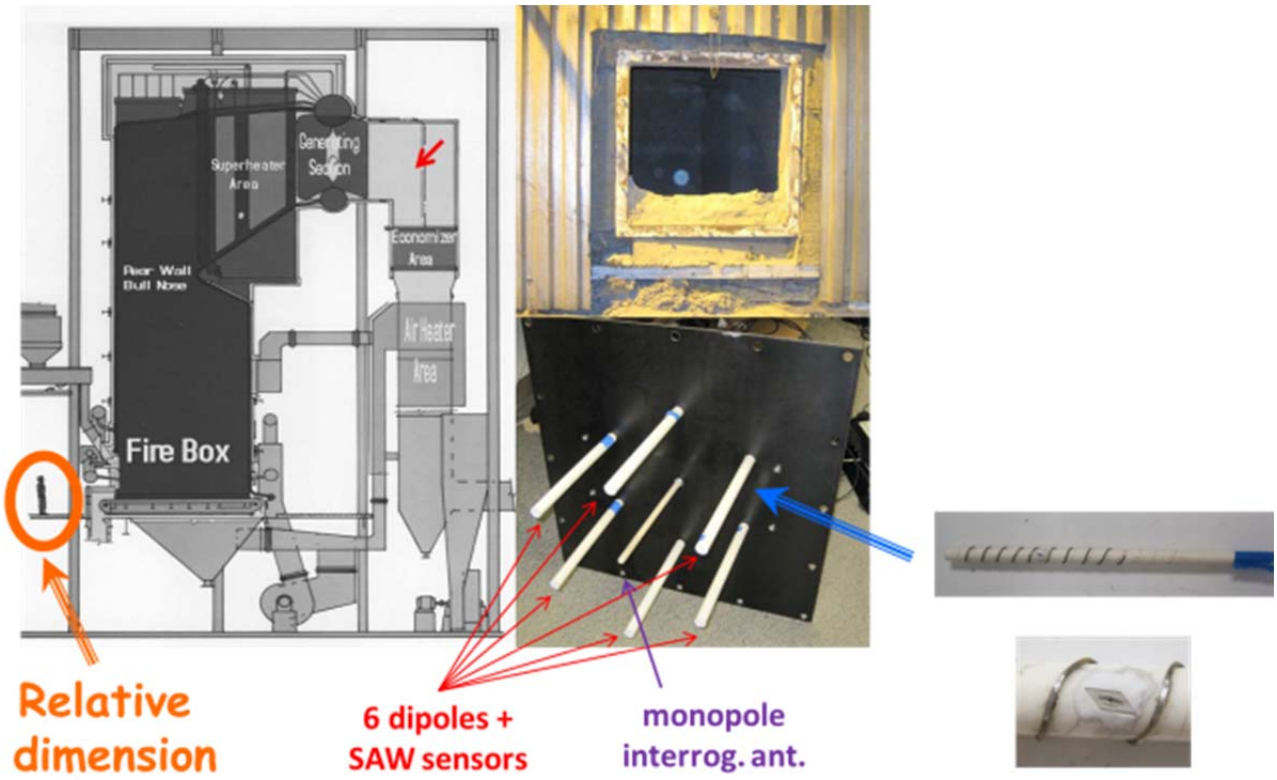

Figure 13: (Left) Schematic showing the PERC power plant facility, the generating section, which contains the boilers, and the economizer area. (Bottom-middle) A six wireless sensor panel array mounted in the economizer point of access shown (Right-top and Left). Also shown in the figure (Bottom-right) are details of the sensor placement, sensor antenna, and overall packaging.

Figure 14 shows the schematic of the PERC power plant facility, highlighting the soot blower locations, boiler and economizer respective locations. The picture on the top-right of Figure 14 shows the back of the boiler tubes seen from the economizer chamber and four wireless SAW sensors and antennas installed. The photo on the bottom of Figure 14 shows an alternate point of installation of a SAW wireless sensor and respective interrogating antenna.

Wireless SAW sensor signal was obtained from these test setups as reported in the next section.

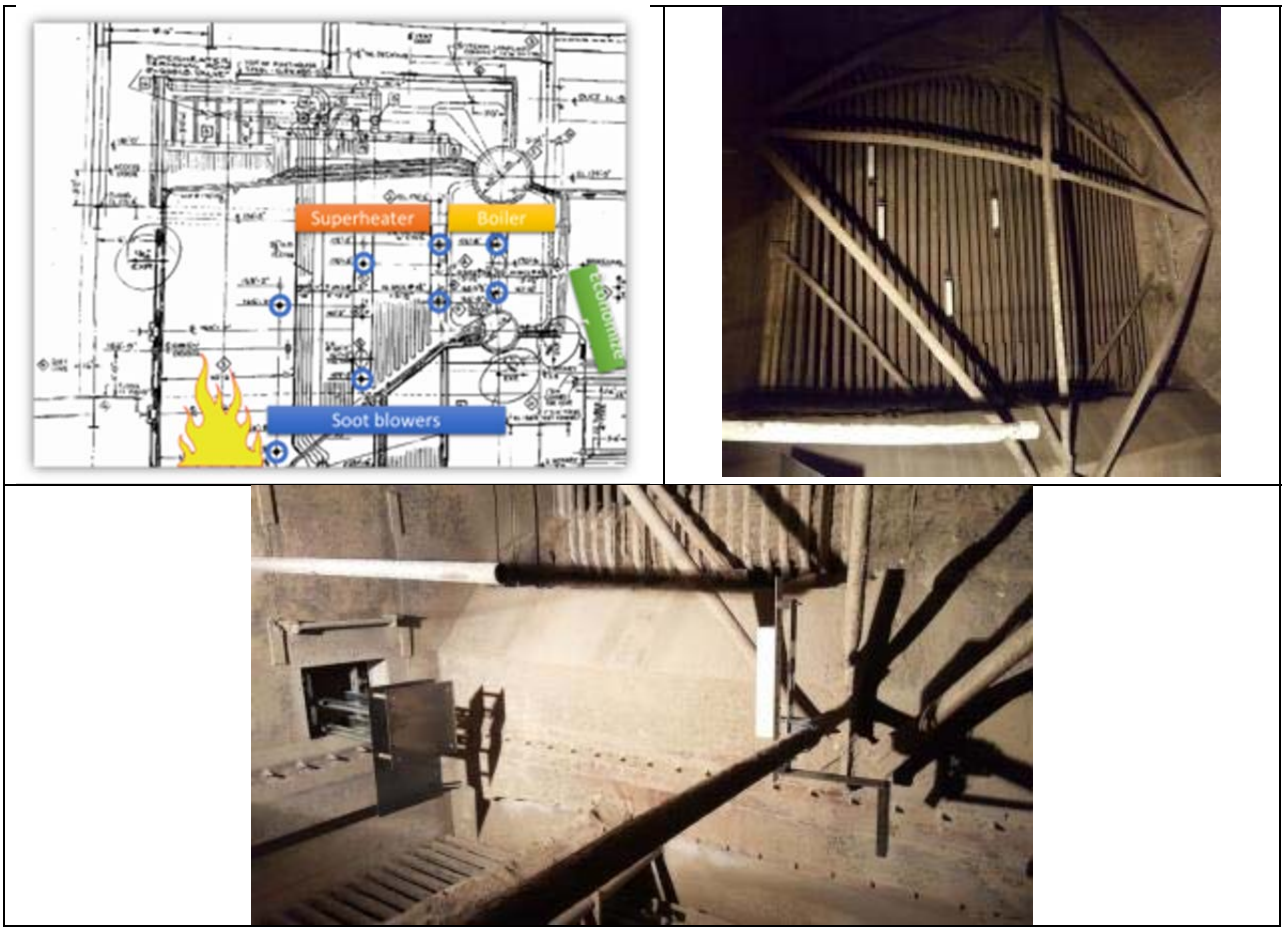

Figure 14: (Top-left) Schematic of the PERC power plant facility, highlighting the soot blower locations, boiler and economizer respective locations. (Top-right) Back of the boiler tubes seen from the economizer chamber with four wireless SAW sensors and antennas installed. (Bottom) An additional wireless SAW sensor installed at the back access point of the boiler tubes and the respective interrogating antenna.

6.2 RESULTS AND DISCUSSIONS

The results presented in this section are a summary of the most relevant achievements throughout the project. For further details on the project results and discussions, the reader is invited to check the published material, listed in Section 8, *References*. Several of the pictures included in this report were used in previous reports and/or used in the publications which resulted from this work, and listed in Section 8 *References*.

6.2.1 Thin Film Research, Development and Performance

Thin-film Electrode Agglomeration

As discussed in *Experimental Methods* Section 6.1 of this report, and depicted in Figure 1 agglomeration is the process by which the metallic thin-film electrode recrystallizes and dewets from the surface where was originally deposited, causing loss of electrical continuity.

Performance of the Pt–Rh/ZrO_2 Electrode

The Pt–Rh/ZrO_2 electrode and respective SiAlON capping layer were used by UMaine and Environetix at the beginning of the project in the fabrication of high temperature SAW sensors. Therefore, an initial task and result to be achieved under this project was the quantification of the performance of this electrode structure as temperatures approached 1000°C.

Figure 15 shows SEM images Pt–Rh/ZrO_2 blanket film of 149 nm thick on LGS after annealing for 4 hours at 1000°C. Figure 15a and Figure 15b SEM images were performed on the bare film and employ secondary electrons detector (SED) and electron backscatter diffraction detector (EBSD), respectively, revealing the strong agglomeration of this type of film upon exposure to 1000°C for 4 hours. Figure 15c and Figure 15d are SEM pictures with the same type of detectors to Figure 15a and Figure 15b, respectively, but now including the SiAlON capping layer used at the beginning of this project. The lighter shaded of gray in Figure 15b and Figure 15d are indicative of the present of elements with a higher atomic number, in this case Pt. As can be inferred from Figure 15, the Pt–Rh/ZrO_2 electrode is not appropriate for long term (> 4 hours) operation at temperature at or above the 1000°C, even considering the SiAlON capping layer to retard the agglomeration process.

The early confirmation about the inadequacy of the Pt–Rh/ZrO_2 electrode and the SiAlON capping layer for long term operation at and above 1000°C, encourage the research and development efforts towards alternative alloys, pinning elements, capping and interfacial layers, which results are summarized next.

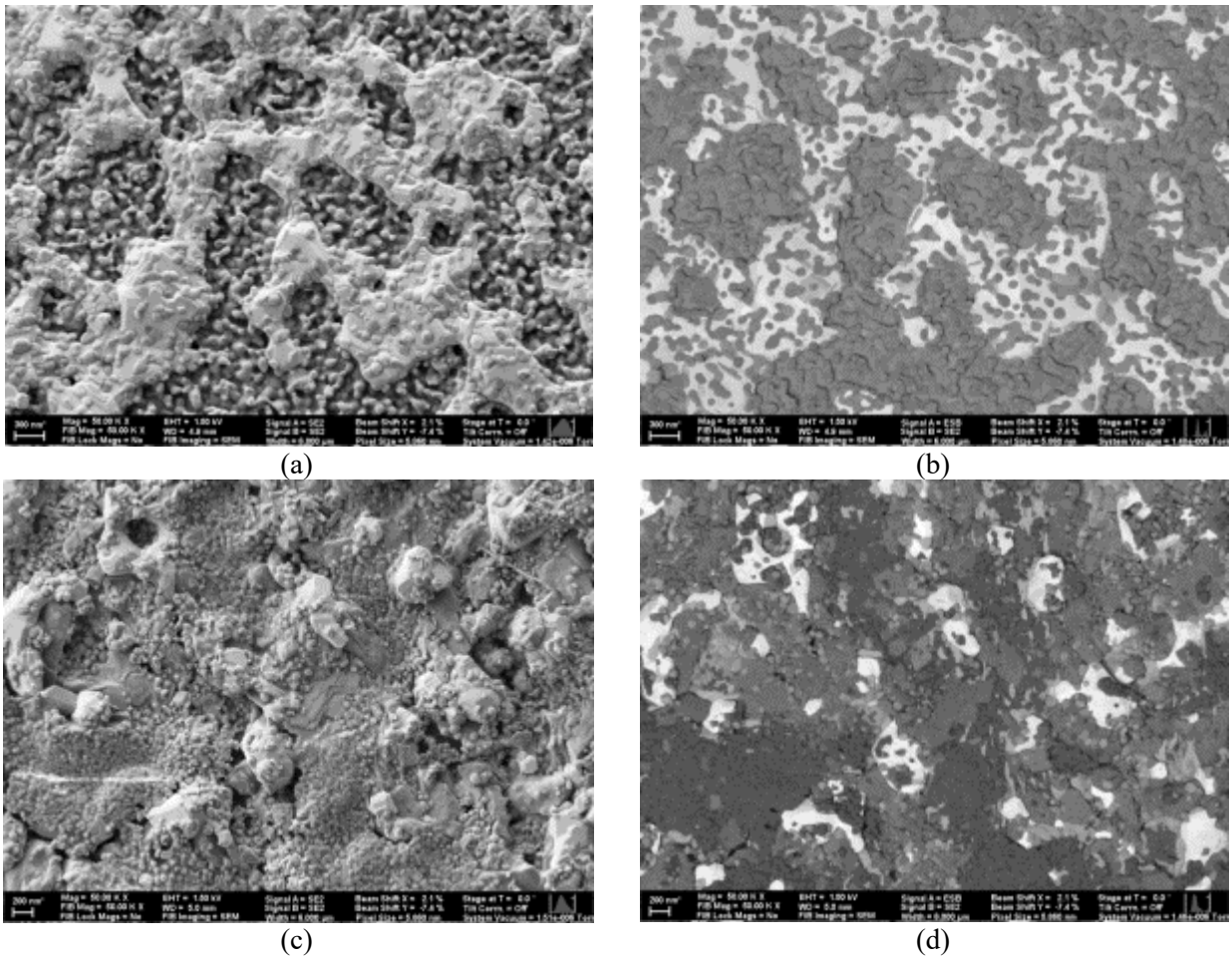

(a) (b) (c) (d)

Figure 15: SEM images of 149 nm thick PtRh/ZrO_2 films on LGS, after annealing for 4 hrs at 1000°C. (a) bare film secondary electrons (SED) (b) bare film electron backscatter diffraction detector (EBSD) (c) SiAlON capping layer (SED) (d) SiAlON capping layer (EBSD)

The Pt–Rh/ZrO_2 Electrode vs. Pt–Rh/HfO_2 Electrode

X-ray diffraction and electron microscopy results indicate that Pt–Rh/HfO_2 films are stabilized by the formation of monoclinic HfO_2 precipitates after high temperature exposure, which act as pinning sites to retard grain growth and prevent agglomeration of the conductive cubic Pt–Rh phase. The Pt–Rh/HfO_2 films were found to be slightly more stable than the Pt–Rh/ZrO_2 films. The Pt–Rh/ZrO_2 films contain both tetragonal and monoclinic ZrO_2 precipitates that also helps prevent Pt–Rh agglomeration.

Pt, Pt–Rh, Pt–Rh/ZrO_2, and Pt–Rh/HfO_2 films Conductivity Results & Analysis

The electrical conductivities of ~150 nm thick Pt, Pt–Rh, Pt–Rh/ZrO_2, and Pt–Rh/HfO_2 films deposited onto langasite substrates were measured at room temperature after air annealing in a tube furnace. The conductivity values were acquired using a four-point probe measurement to eliminate contact resistances. Each data point in Figure 16 represents the conductivity measured following annealing for 4 h at the given temperature. Although the Pt and Pt–Rh films have

about 2½ times higher conductivity than the nanocomposite films at 800 °C, they show a loss of conductivity and failure at temperatures above 800 and 900 °C, respectively, due to recrystallization and agglomeration. The Pt–Rh/HfO2 nanocomposite film maintained a conductivity >1 × 106 S/m up to 1,000 °C and 7 × 105 S/m after 4 h at 1,050 °C. It failed following annealing at 1,100 °C as evidenced by a lack of electrical continuity. The Pt–Rh/ZrO2 film was slightly less stable, remaining conductive after 4 h at 1,000 °C but failing after heating to 1,050 °C.

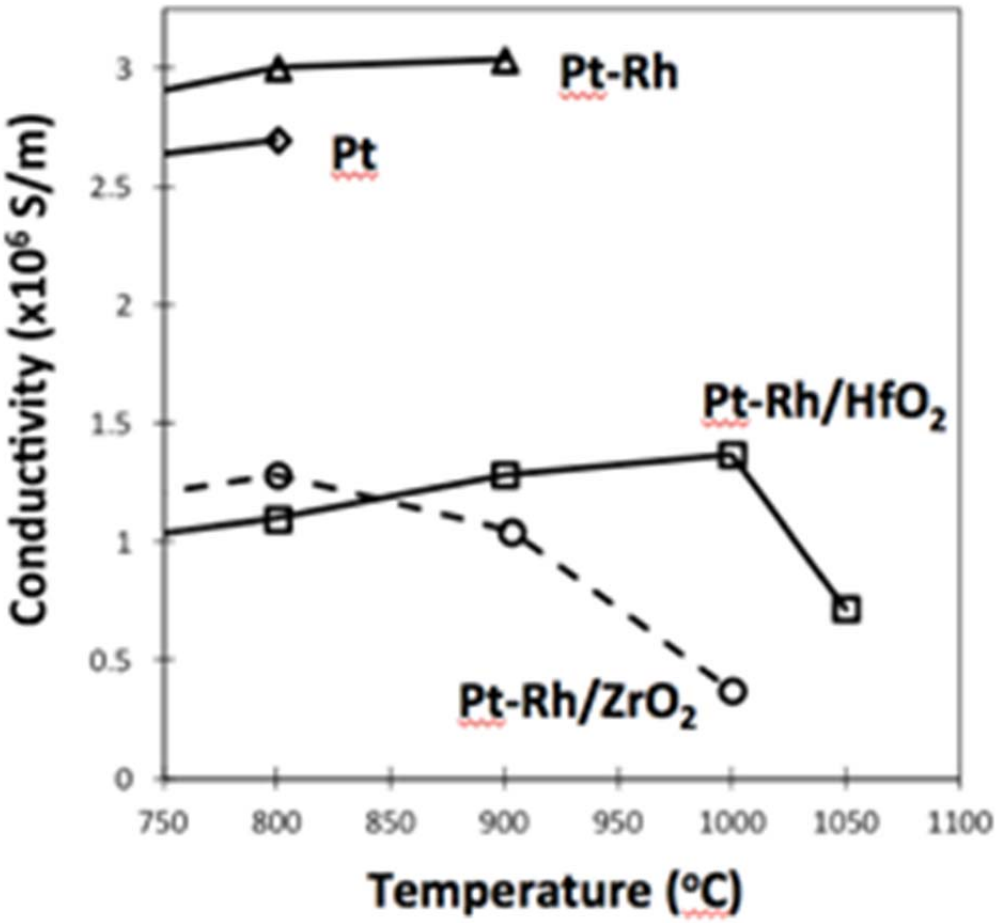

Figure 16: Room temperature electrical conductivity measured from 150 nm thick films deposited onto langasite substrates after annealing for 4 h at the indicated temperature. The films degraded and the conductivity went to zero at tested temperatures higher than the last data point shown for each film type. Measurements were taken after annealing at the following temperatures: 800, 900, 1,000, 1,050, and 1,100 °C

SiAlON Capping Layer vs. ALD Al_2O_3 Capping Layer

As discussed above in this section, additional film stability can be achieved by adding a thin "capping" passivation film over the Pt–Rh/HfO_2 film surface. Previous work with Pt–Rh/ZrO_2 electrodes has shown that the incorporation of a thin oxynitride (SiAlON or SiZrON) coating over the entire sensor diminishes high temperature roughening and degradation of both the electrode and bare langasite surfaces up to 1,000°C.

At temperatures above 1,000°C, however, the SiAlON coating begins to degrade and is no longer effective at hindering agglomeration. The presence of Si in the SiAlON capping layer showed to be detrimental to high temperature operation above 950°C, by fostering the formation of Pt silicides and to the possible decomposition of the oxynitride resulting in the enhanced oxidation of the Pt and loss of volatile PtO_2.

Figure 17 shows SEM secondary electron images from Pt–Rh/HfO_2 films covered with 50 nm thick capping layers after annealing at 1,050 °C for 4 hours, using ALD alumina capping layer (Figure 17a) and SiAlON capping layer (Figure 17b).

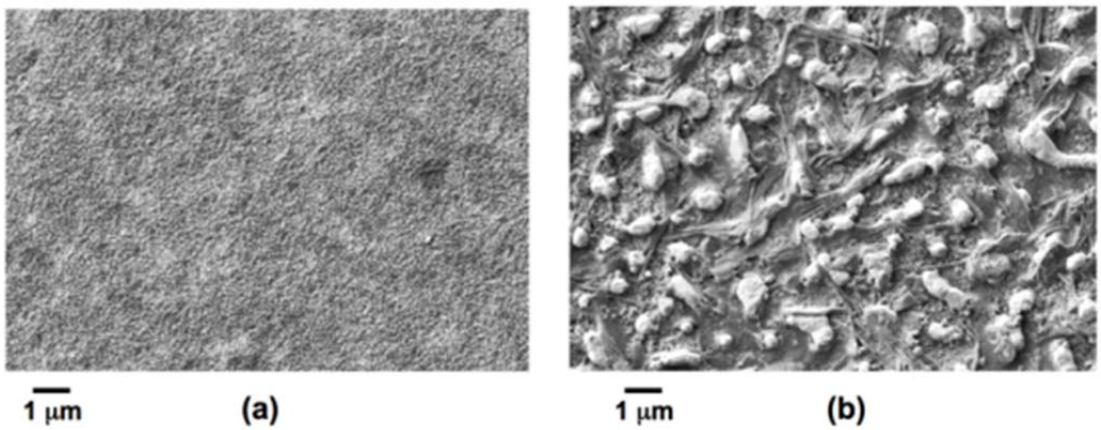

Figure 17: SEM secondary electron images from Pt–Rh/HfO2 films covered with 50 nm thick capping layers after annealing at 1,050 °C for 4 h: an ALD alumina capping layer and b SiAlON capping layer

The use of an ALD-grown Al_2O_3 layer is found to be much more stable above 1,000°C. Using the ALD alumina approach, a stable film electrical conductivity is retained at least to 1,100°C as shown by the "star" data point in Figure 18.

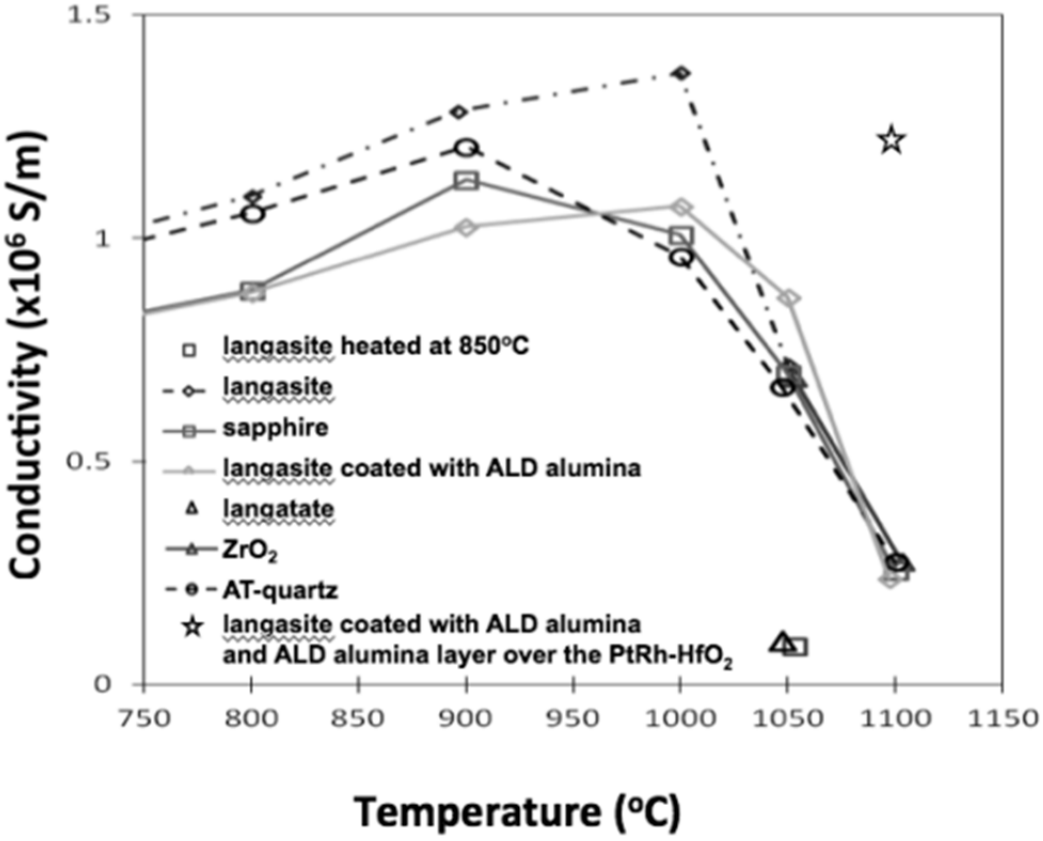

Figure 18: Electrical conductivity measured from 150 nm thick Pt–Rh/HfO2 films deposited onto different substrates, after annealing for 4 h at the indicated temperatures

Other Substrates and Interfacial Layer

In addition to showing the effect of the ALD Al_2O_3 capping layer on the performance of the thin electrode film, Figure 18 also reveals the effect of the deposition of the electrode films on top of different substrates. In particular, the deposition on top of LGS

In order to investigate whether La and/or Ga diffuses out of the langasite substrate and reacts with the nanocomposite film, Pt–Rh/HfO_2 films were deposited onto a variety of different substrates and film conductivity was measured after 4 h at a given temperature as shown in Figure 18. There is a loss in conductivity after annealing at 1,050 °C for the langasite substrate, and the failure is even more pronounced for a langatate substrate and a langasite substrate that was pre-annealed at 850°C. However, improved survivability is shown for Pt–Rh/HfO2 films on sapphire, AT-quartz, ZrO_2, and langasite coated with 50 nm of alumina grown by the ALD process. The fact that all the substrates that do not contain La or Ga remain conductive to 1,050°C and show similar behavior, suggests that diffusion of Ga or La into the nanocomposite film above 1,000°C occurs and is detrimental to the film stability.

Figure 19 shows SEM backscatter images of the Pt–Rh/HfO_2 films deposited on the different substrates after heating at 1,050°C for 4 h. The film morphologies are consistent with the conductivity results, namely that less agglomeration is visible on substrates that do not contain La or Ga which yields a more stable conductivity behavior. It is also interesting to note that the morphologies of the Pt–Rh/HfO_2 films grown on single crystal sapphire and ALD alumina-coated LGS are very similar, illustrating the effectiveness of Al_2O_3 in minimizing interdiffusion and film agglomeration.

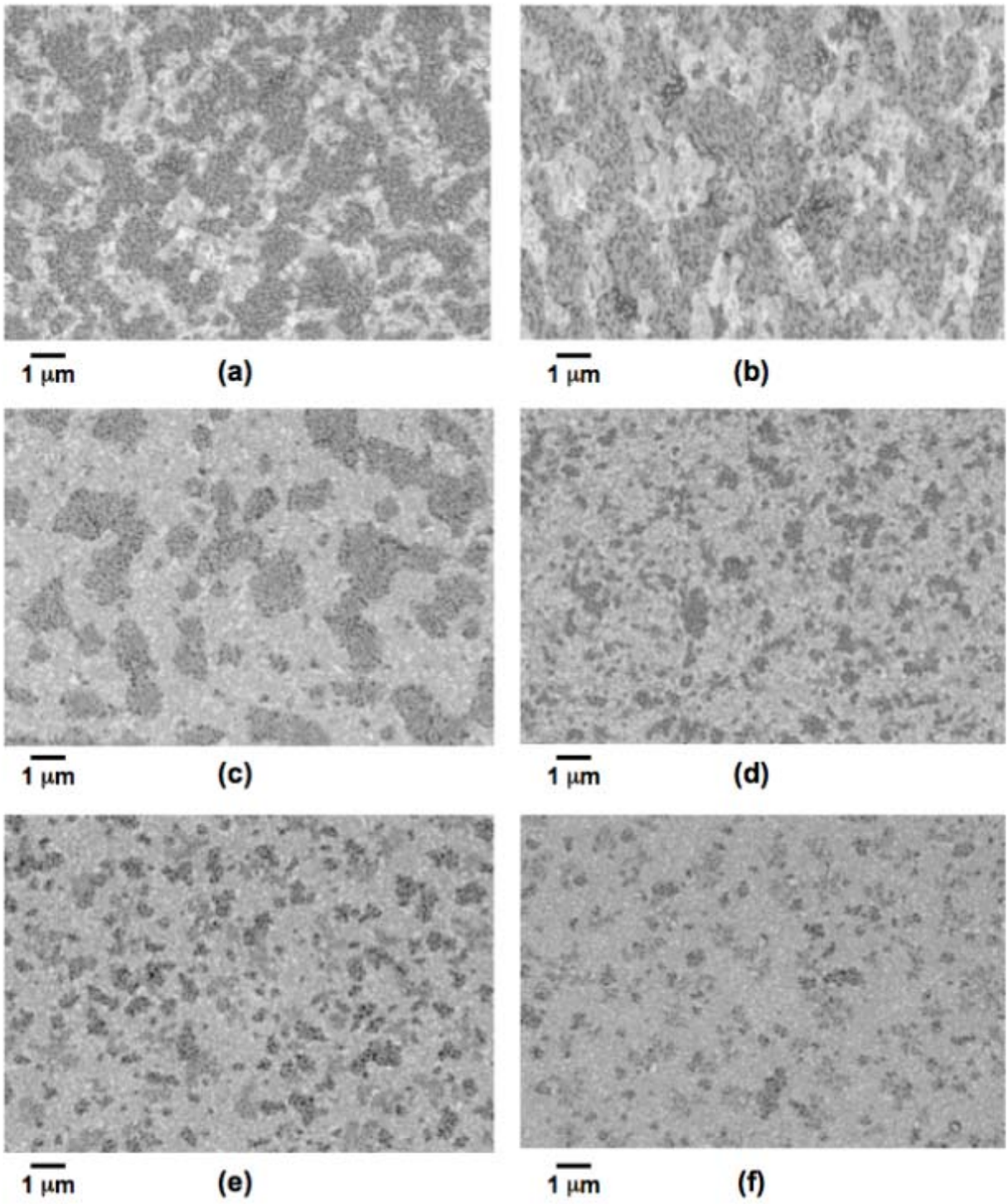

Figure 19: SEM backscatter images of Pt–Rh/HfO2 films deposited onto different substrates and heated in air at 1,050 °C for 4 h: (a) langasite annealed for 4 h at 850 °C prior to Pt–Rh/HfO2 deposition, (b) as-polished langatate, (c) as-polished langasite, (d) ZrO2 single crystal, (e) r-cut sapphire, and (f) langasite covered with 50 nm ALD alumina layer.

Other Types of films Studied & Performance

Other Pt-alloys

A wide range of 150 nm thick Pt-alloy films containing a dispersed oxide phase (TiO2, Ta2O5, Nb2O3, Al2O3, RuO2, SnO2, CoO, Cr2O3, NiO, SiO2, ZrO2, Y2O3, HfO2, CeO2, MnO2) were screened for their electrical conductivity after annealing up to 1200 °C in air. The films were deposited onto sapphire and langasite substrates coated with a 10 nm thick adhesion layer (Cr, Nb, Hf, Y, Mn, Ni, CeOx) using e-beam co-evaporation in both vacuum and in background O2 gas. Following air heat treatments up to 1200 °C, all the metallic components completely oxidized into a second phase oxide that coexists with Pt-rich grains. The film structure is essentially the one depicted in Figure 8. The multilayer architecture implemented consists of a 150 nm thick conducting Pt-alloy electrode inserted between a 10 nm thick adhesion layer and a 50 nm-thick protective capping layer on sapphire or langasite substrates.

As previously mentioned in this report, second phase inclusions or interlayers within the Pt-alloy films provide grain boundary pinning and hinder agglomeration of Pt grains, resulting in films that retain conductivities larger than 1×10^6 S/m after annealing in air. Pt–Al_2O_3, Pt–HfO_2, and nanolaminate Pt–Ni/Pt–Zr films performed the best, remaining conductive after annealing to 1050–1150°C. For Pt–Rh/HfO_2 films, adhesion layers of Ni, Zr, Y, and CeOx yielded the highest film stability temperature.

Figure 20 shows the results of conductivity measurements at room temperature of various Pt-alloy electrode films investigated under this project on both sapphire (Figure 20a) and langasite (Figure 20b) substrates after heating in air for 4 h at the indicated temperatures, along with data for a pure Pt and $Pt_{83}Rh_{17}$ film for reference. The electrode films were 150 nm thick with a 10 nm Zr adhesion layer, and alloy compositions are given in atomic percent.

The $Pt_{50}Si_{50}$ and $Pt_{83}Ru_{17}$ films failed after initially heating to 800 °C and are not shown in Figure 20. The $Pt_{86}Al_{14}$ film was the best film and remained conductive to 1100 °C on langasite. The Pt85Nb15, Pt80Sn20, and Pt85Co15 alloy films show promise, having survived to temperatures equal to or higher than the reference $Pt_{83}Rh_{17}$ film. The $Pt_{85}Co_{15}$ and $Pt_{90}Ni_{10}$ alloys deposited on sapphire had the same maximum survival temperature as $Pt_{83}Rh_{17}$ on langasite, with the additional benefit of higher conductivity. Increasing the Ni content up to $Pt_{70}Ni_{30}$ extended the film operational temperature range, although film conductivity was reduced by about a factor of two. Films that did not perform as well as the reference $Pt_{83}Rh_{17}$ film, failing after heating at 900 °C, included $Pt_{90}Cr_{10}$, $Pt_{94}Ti_6$ and $Pt_{96}Ta_4$ as well as the pure Pt film.

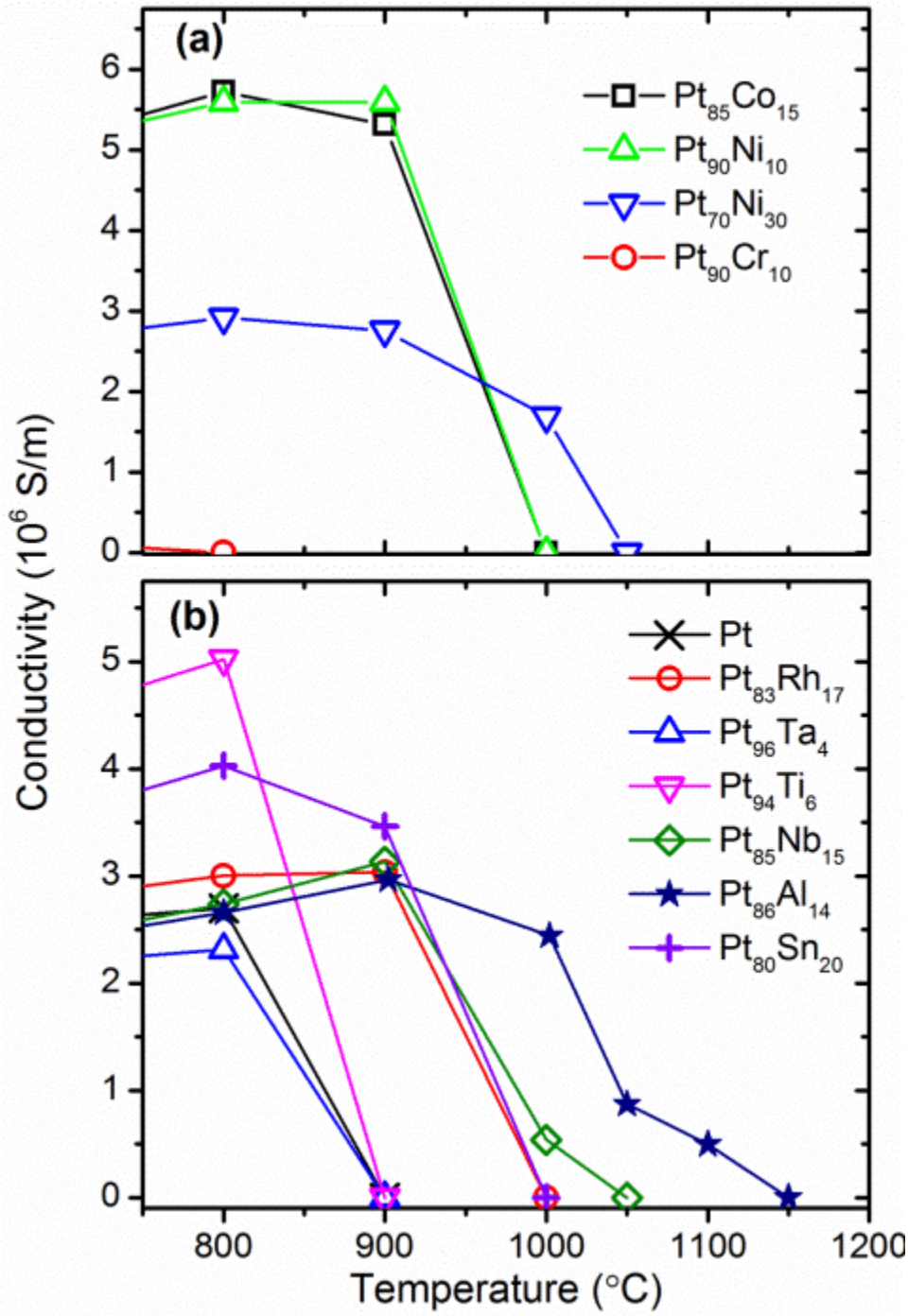

Figure 20: Room temperature electrical conductivity of various Pt-alloy electrode films on (a) sapphire and (b) langasite substrates after heating in air for 4 h at the indicated temperatures. The electrode films were 150 nm thick with a 10 nm Zr adhesion layer, and alloy compositions are given in atomic percent.

Other Pinning Materials

The effect of using different types of metal oxide inclusions for grain boundary pinning and high temperature stabilization of Pt-alloys was studied. Figure 21a shows the conductivity results for seven prospective pinning materials: MnO_2, CeO_2, NiO, HfO_2, CoO, Al, and ZrC added to $Pt_{83}Rh_{17}$ films on sapphire substrates. Previous work has shown that incorporating ZrO_2 into $Pt_{83}Rh_{17}$ films at levels corresponding to 10–28 at. % Zr as determined by XPS, can extend the conducting range of $Pt_{83}Rh_{17}$ films up to 1000°C via formation of ZrO2 inclusions that help stabilize the film morphology. Based on these results, a ratio of the pinning metal concentration to Pt concentration of 27% was targeted in this project.

On sapphire substrates (Figure 21a), HfO_2 proved to be the best pinning additive, with the film remaining conductive up to 1150°C, which is 50 °C higher than the same film on a langasite substrate. Films with Al and MnO2 failed at a 50 °C lower temperature than the film with HfO_2, with performance similar to films with ZrO_2 as a pinning additive. Interestingly, the $Pt_{83}Rh_{17}$–Al film in these tests did not perform as well as the Pt/Al_2O_3. The presence of Rh is evidently associated with the earlier failure of the $Pt_{83}Rh_{17}$–Al film. The film with CeO_2 as an additive failed after heating at 1050 °C, and films with ZrC, CoO and NiO inclusions did not perform as well, failing after heating at 1000°C. Although carbides are attractive due to their high temperature performance and alternate chemistry as opposed to oxides, the sample with ZrC as a pinning material was only conductive to 900 °C, possibly due to oxidation of the ZrC phase at higher temperatures.

On langasite substrates (Figure 21b), the $Pt_{83}Rh_{17}$ film with no pinning additives, labeled 'None' in Figure 21b, was conductive after heating to 900 °C and failed after heating to 1000°C, whereas the $Pt_{83}Rh_{17}$–ZrO_2 reference material remained conductive after heating to 1000°C and failed after heating at 1050°C, consistent with previous work. Co-deposition of Zr in the absence of oxygen resulted in a film that performed very similar to a film co-deposited with Zr in a 2.7×10^{-3} Pa O_2 background pressure, again signifying that inclusions of the maximum valence oxide, ZrO2, are formed during the high temperature air anneal. Results from other films deposited on langasite substrates indicate that (i) films with Nb_2O_3 and RuO_2 are inferior compared to samples containing ZrO_2, (ii) films with Y_2O_3 have a similar failure temperature and somewhat higher conductivity, and (iii) films with HfO_2 have a higher survival temperature by approximately 50°C. Replacement of Zr by Ru caused the film to fail at 1000°C, likely due to the higher vapor pressure of RuO_2. Niobium has atomic number that is one larger than Zr and a higher melting point, but use of Nb_2O_3 as a pinning material also resulted in failure at 1000°C. Yttrium has an atomic number one lower that Zr, and Y_2O_3 has been used for pinning in bulk Pt-based materials and phase stabilization of zirconia. Use of Y_2O_3 resulted in higher conductivity at 900 °C and 1000 °C, but did not extend the survivability to higher temperatures. Hafnium has very similar chemical properties to Zr, but twice the mass and hence Hf has lower atomic mobility. The replacement of Zr with Hf resulted in increased film conductivity at 900 °C and 1000°C and a 50°C increase in the maximum temperature at which the film remained conducting.

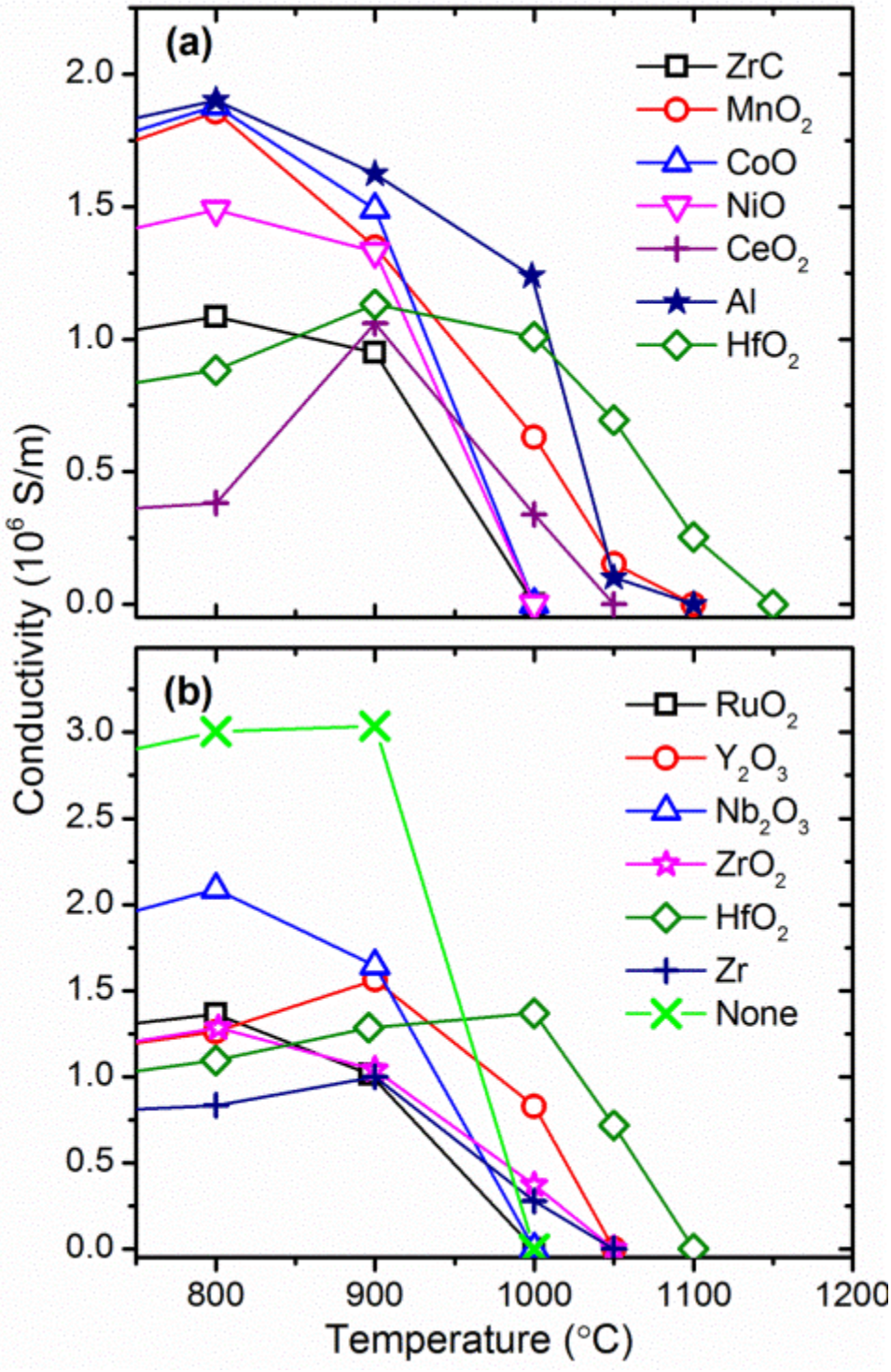

Figure 21: Electrical conductivity of $Pt_{83}Rh_{17}$ films co-deposited with different grain boundary pinning materials after heating for 4 h in air at the indicated temperatures: (a) on sapphire substrates with Zr adhesion layer, and (b) on langasite substrates with Zr adhesion layer.

Summary Regarding High-Temperature Pt-alloys and Pinning Materials

Metallic conducting electrode films tend to either agglomerate into isolated islands or become heavily oxidized at high temperature in air leading to insulating behavior. A wide range of 150 nm thick Pt-alloy films containing a dispersed oxide phase (TiO_2, Ta_2O_5, Nb_2O_3, Al_2O_3, RuO_2, SnO_2, CoO, $Cr2O_3$, NiO, SiO_2, ZrO_2, Y_2O_3, HfO_2, CeO_2, MnO_2) were screened for their electrical conductivity after annealing up to 1200 °C in air. The films were deposited onto sapphire and langasite substrates coated with a 10 nm thick adhesion layer (Cr, Nb, Hf, Y,Mn, Ni, CeOx) using e-beam co-evaporation in both vacuum and in background O_2 gas. Following air heat treatments up to 1200 °C, all the metallic components completely oxidized into a second phase oxide that coexists with Pt-rich grains. Layering or adding oxide inclusions provides grain boundary pinning and hinders the agglomeration process to achieve electrical and morphological film stabilization. The best performing electrode films that were tested in this study were Pt–Al_2O_3, Pt–HfO_2, and Pt–Ni/Pt–Zr nanolaminate films, which retained conductivity after heating in the 1050–1150 °C range.

6.2.2 SAW Sensor Performance at High Temperature

Agglomeration on Transducer Electrodes

All the thin-film electrode results discussed in the previous Section 6.2.1 apply for the electrodes built on top of LGS for SAW device, but one extra phenomenon is worth mention, a phenomenon highlighted when IDTs or finite width reflector electrodes are fabricated. The agglomeration phenomenon discussed in Section 6.2.1 and which is based on the recrystallization of the Pt material often leads to the shrinking of the Pt–Rh/ZrO_2 electrodes, as shown in Figure 22. This electrode shrinkage is highly undesirable for a SAW device operation, since it changes the performance of the SAW sensor, leading to drifting and ultimately its failure. The measures discussed in the previous section, namely the capping and the interfacial layer were very important to diminish this phenomenon as temperature was increase to the limit of the electrode material, by making the agglomeration more uniform in the electrode region.

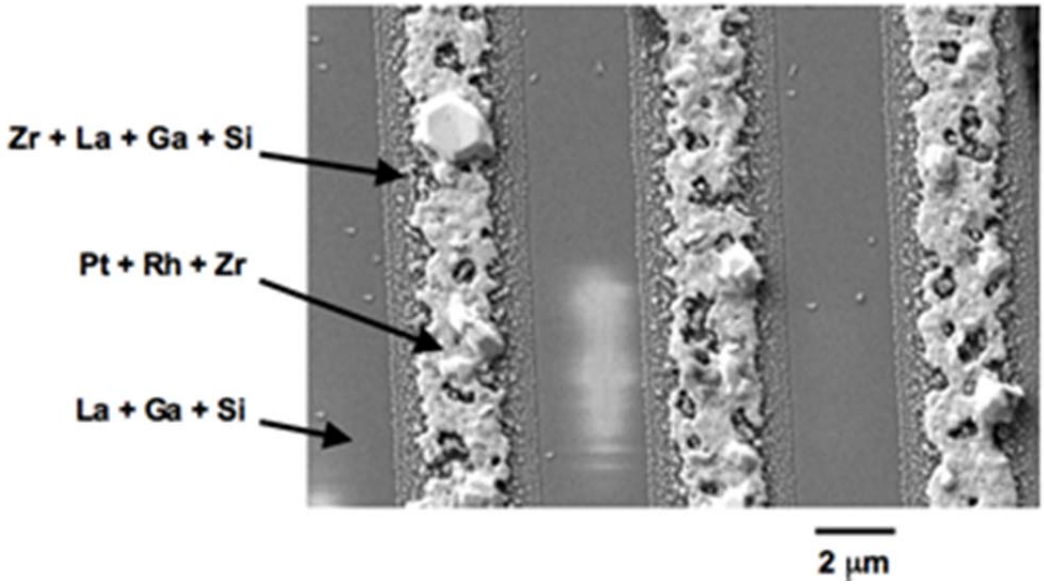

Figure 22: SEM secondary electron image showing morphological changes of photolithographically patterned 2 μm wide Pt–Rh/ZrO_2 finger electrodes on a langasite substrate after annealing in air at 900°C for 16 h. The initial electrode thickness was 120 nm.

Another phenomenon observed in the case of Zr|Pt-86/Al-14 electrodes with thicknesses around 180nm. Figure 23 shows SEM images for four similar PtAl devices heated for 4 hours at (a) 900°C, (b) 1000°C, (c) 1050°C, (d) 1100°C. As can be seen from the figures, the border of the electrodes, which due to the metal deposition during the fabrication received low quantities of Al, and most of Pt, have more severe agglomeration and hillock formation. Also seen in this figure is that at 1100 ºC, the Pt in the electrodes agglomerated to the point where there is no electrical continuity in the interdigitated (IDT) transducers.

Figure 24 shows the absolute value of the S_{11} scattering parameter, $|S_{11}|$, frequency response for 4 similar SAW resonator devices, each measured before annealing (blue solid line); after annealed at 850ºC for 4 hours (magenta dashed line); and after exposure to different high temperature values (green dotted lines). The green dotted lines show the response of the four devices after heating for 4 hours at 900ºC, 1000ºC, 1050ºC and 1100ºC, respectively. It is evident from the plots that the devices deteriorated with increasing temperature. Devices heated at 1100ºC and above did not show any response after heating, which is consistent with the SEM pictures shown in Figure 23.

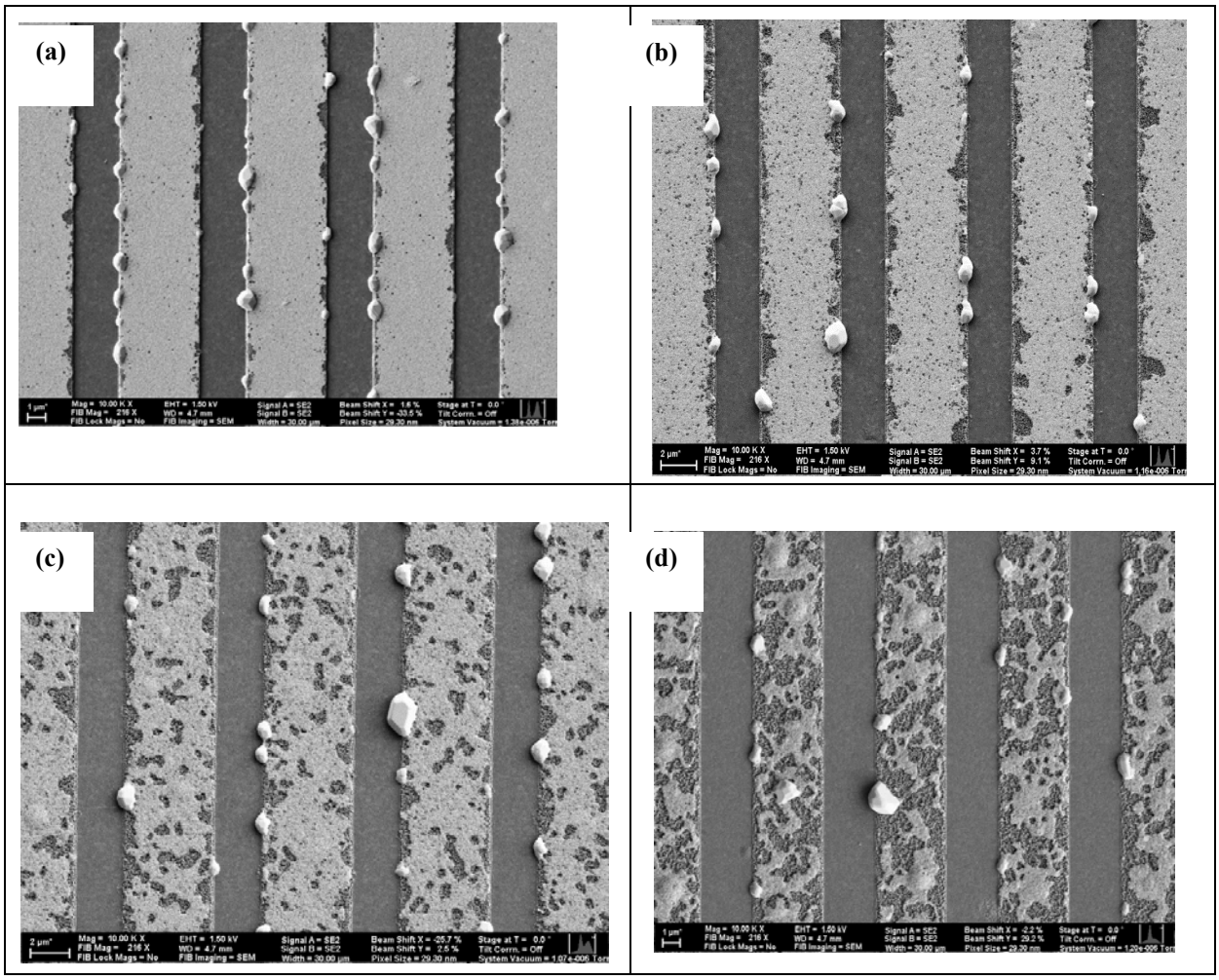

Figure 23: SEM images of devices heated for 4 hours at (A) 900°C, (B) 1000°C, (C) 1050°C, (D) 1100°C.

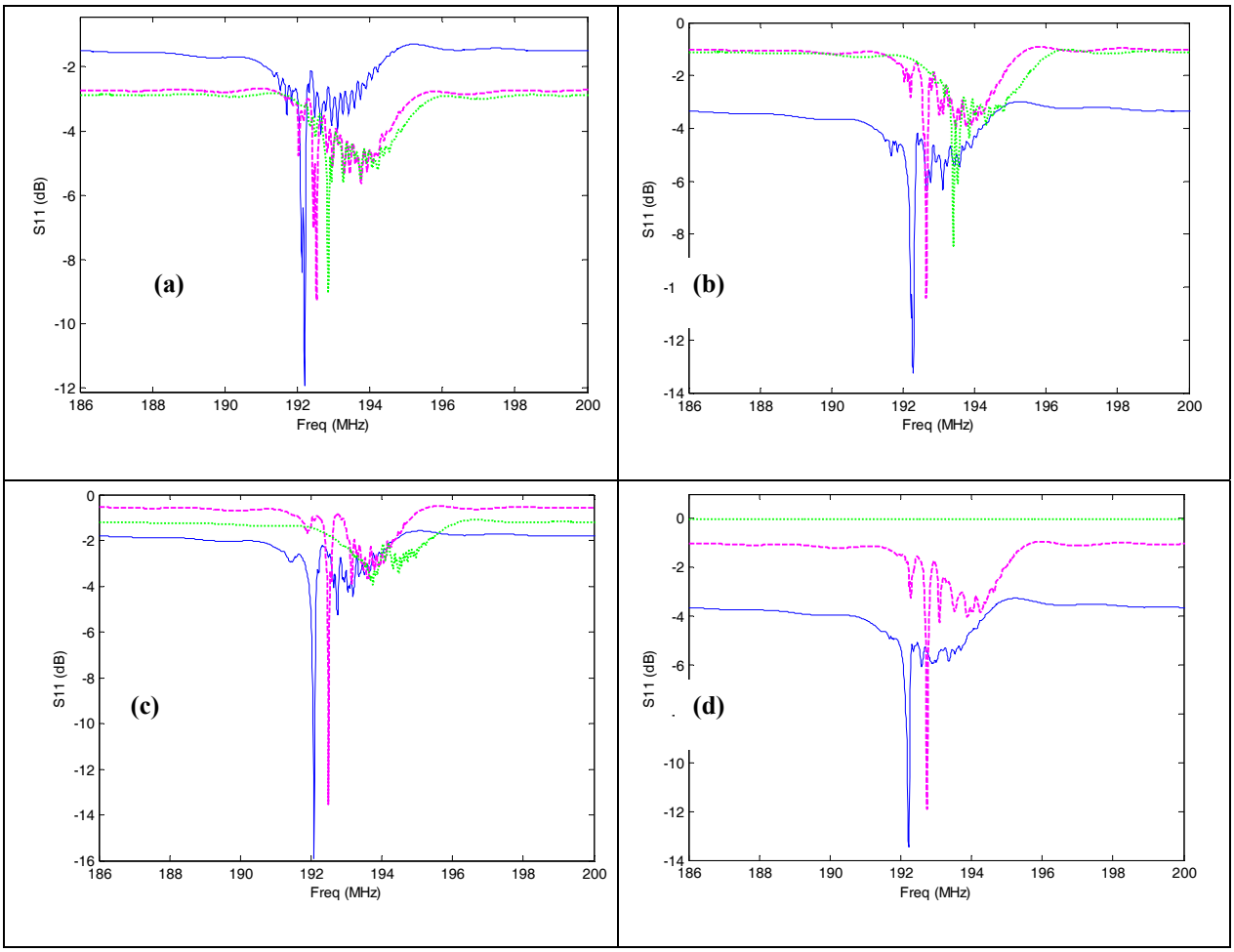

Figure 24: Response of a SAW resonator with Pt-Al electrodes before annealing (solid-blue) and after 850°C annealing (dashed– magenta) and after further heating (dotted-green) to (a) 900°C; (b) 1000°C; (c) 1050°C; and (d) 1100°C.

Whiskers

Another issue encountered in the fabrication and testing of [LGS]Zr|PtRh/ZrO_2 co-deposited electrode device was the formation of whiskers. As the devices were annealed to functionalize the electrode, it was verified that the IDTs were being short-circuited following the heating treatments. Examination of the shorted devices with the SEM indicated that whiskers or nanowires were forming during high temperature annealing steps and laying across the fingers to cause the short circuit behavior electrically identified. As shown in the upper left image in Figure 25a, the whiskers appear to grow from the centers of mounded high stress features that develop during annealing. Hillocks were also observed to form at center of the mounds.

Multilayer films were grown with 4 bi-layers of PtRh alloy and ZrO_2 in which the overall PtRh: ZrO_2 composition ratio was the same as the co-deposited material. In these samples, Figure 25b, the whiskers were observed to be shorter and thinner than for the co-deposited material. When an ALD alumina cap was grown on top of the multi-layer devices no whisker formation was

observed at all, Figure 25c. It was found that vacuum annealing also eliminated whisker growth, Figure 25d. However, this treatment led to pitting of the LGS surface, likely due to loss of Ga from the surface region. It was concluded that for devices with PtRh-based electrodes capping the devices with alumina was an effective method of avoiding the shorting behavior and that for un-capped devices other strategies would have to be used such as forming multi-layered electrodes.

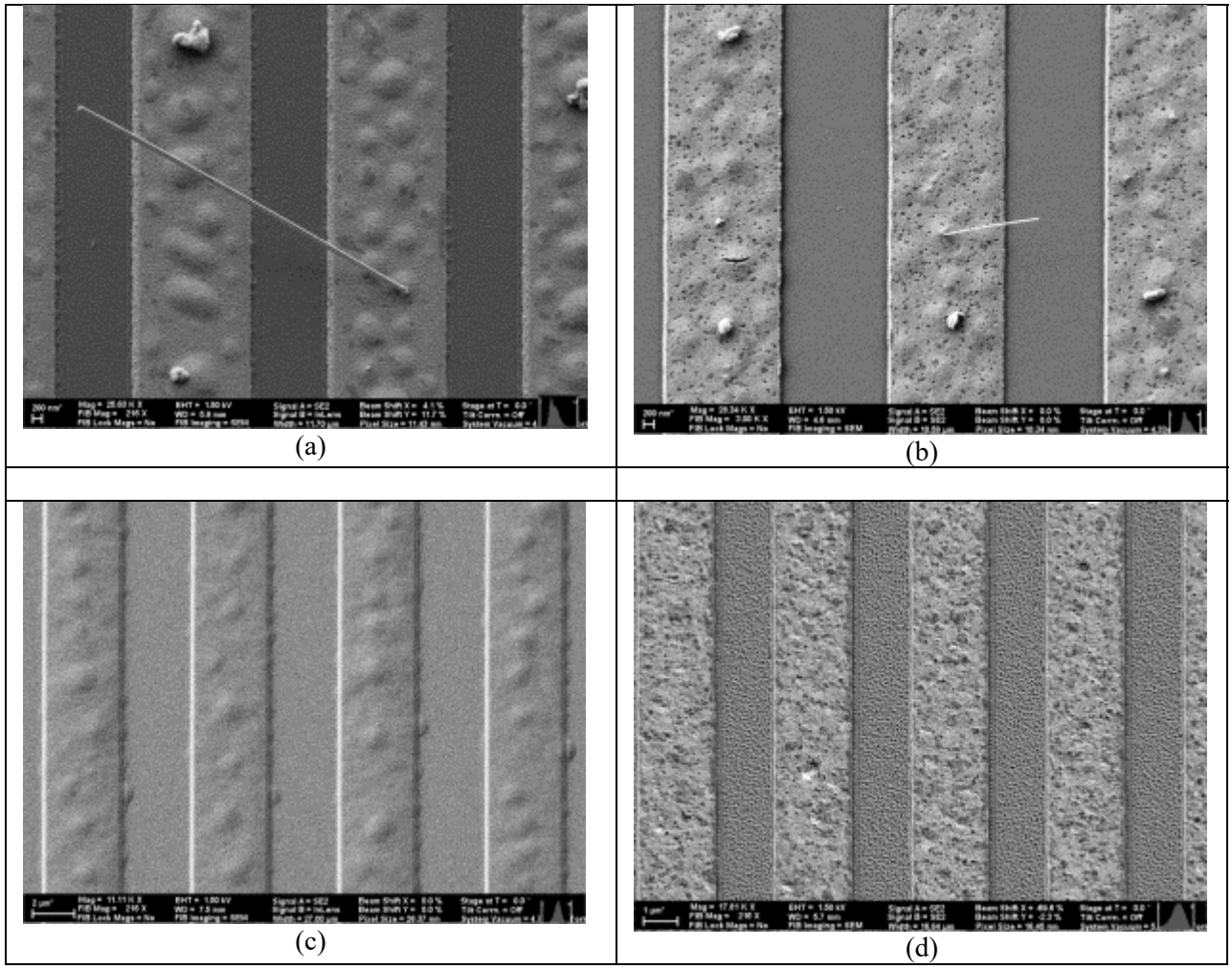

Figure 25: SEM images of: (a) [LGS]Zr|PtRh/ZrO_2 codeposited device; (b) [LGS]Zr[PtRh|ZrO_2]x4 multilayer device; (c) [LGS]Zr[PtRh|ZrO_2]x4|Al_2O_3 multilayer device with alumina cap; (a), (b), and (c) were air annealed at 850°C for 4 hours; (d) [LGS]Zr[PtRh|ZrO_2]x4 multilayer device vacuum-annealed at 850°C for 4hrs.

High-Temperature: Long-term Exposure & Cycling

The temperature profile shown in Table 1 was utilized to test SAW devices with different types of electrodes and film architectures. An Anritsu portable vector network analyzer controlled by a laptop and LabView data acquisition software was configured to measure the scattering parameter S_{11} as a function of process temperature. The tests used a computer controlled high temperature box furnace capable of operating up to 1100°C. The test fixture used for these tests has been shown in the description of the experimental methods, Section 6.1.2, Figure 7.

Table 1: Temperature profile used for Pt-Rh/HfO_2 co-deposited IDTs with an ALD Al_2O_3 interfacial layer

Temperature (°C)	Duration (hours)
350	0.15 (≈ 10 min)
550	0.15
750	0.15
800	0.15
900	2
950	3
1000	3
1050	3
1100	3

In addition to the finite test period defined in Table 1, long term tests were also carried out with Pt-Rh/HfO_2 resonators at 1050°C. After reaching 1050°C, the devices were held at that temperature until failure to check the survivability of these resonators at 1050°C.

Table 2 shows the high temperature performance of the several Pt-based electrode types and film structures used for the LGS SAW resonators operated up to 1100°C. The fourth column in the table indicates the presence or absence of the ALD Al_2O_3 interfacial layer. The fifth column shows the maximum temperature achieved by a particular SAW resonator and the maximum time it operated at that temperature. All devices reported in Table 2 were capped with a 50 nm thick ALD Al_2O_3 layer.

Table 2: High-temperature SAW resonator performance for different IDT electrode compositions

	Resonator film type	Film deposition method	ALD Al_2O_3 interfacial layer	Max temp (°C) & time (minutes)
1	Pt-Rh/ZrO_2	Co-deposition	No	1050 for 120
2	Pt-Rh/ZrO2	Co-deposited	Yes	1050 for 160
3	Pt/Al_2O_3	Co-deposition	No	1050 for 10
4	Pt/Al_2O_3	Co-deposition	Yes	1050 for 70
5	Pt-Rh|HfO_2	Multilayer	No	1050 for 120
6	Pt-Rh|HfO_2	Multilayer	Yes	1050 for 180
7	Pt-Rh/HfO_2	Co-deposition	Yes	1100 for 90
8	Pt-Rh/HfO_2	Co-deposition	Yes	1100 for 130

Figure 26 shows SAW resonator center frequency response as a function of time for a SAW sensor similar to the ones shown in rows 7 and 8 of Table 2. Instead of bringing the device to 1100°C, in this case the device was kept at 1050°C until failure. The dashed line shows changes in temperature measured by the thermocouple, and the solid line shows the changes in the SAW resonator center frequency. The device survived 12 hours at the maximum temperature of 1050°C. At the failure temperature, degradation occurs in the form of reduction in resonator quality factor, significant changes in impedance, and change in the resonant frequency. The upward drift during the 1050°C temperature hold corresponds to a frequency variation of 270 KHz. About half of this drift occurred during the last 2 hours of the test due to the onset of IDT electrode deterioration.

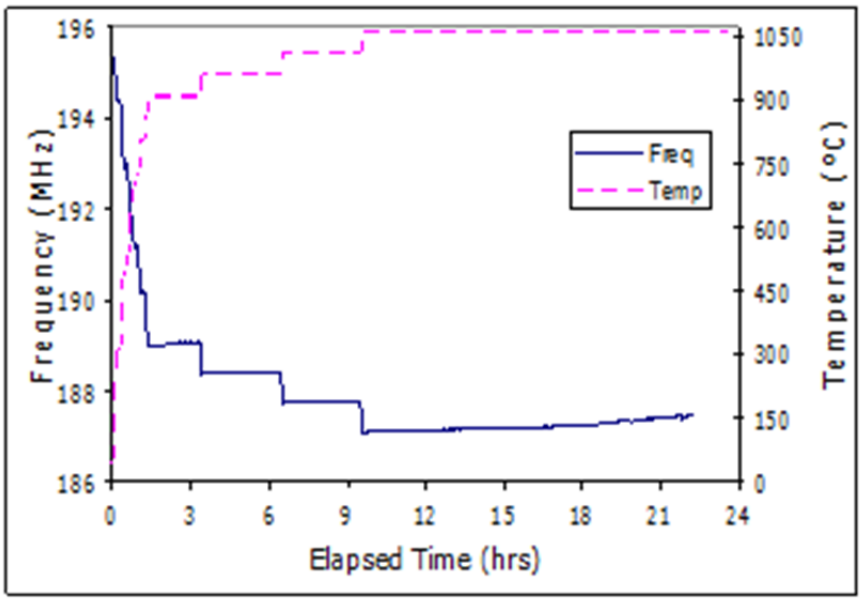

Figure 26: Resonant frequency response versus time for a SAW resonator employing Pt-Rh/HfO_2 co-deposited IDT electrodes

It should be noted electrode stability, including thin and thick paste film in the region of the bus-bars (bondpads), at temperatures approaching 1200°C is challenged by the strong thermodynamic driving forces that cause film agglomeration and interdiffusion phenomena in this temperature regime. In particular, for the Pt-based alloy films studied, it was verified that Pt volatizing in air environment approaching 1200°C is significant, even considering the successful alloy elements that deter the agglomeration. Once the Pt agglomeration takes place, then the Pt volatizing in air is accelerated. This phenomenon was also observed for the Pt thick paste used for the contacts, as shown in Figure 27.

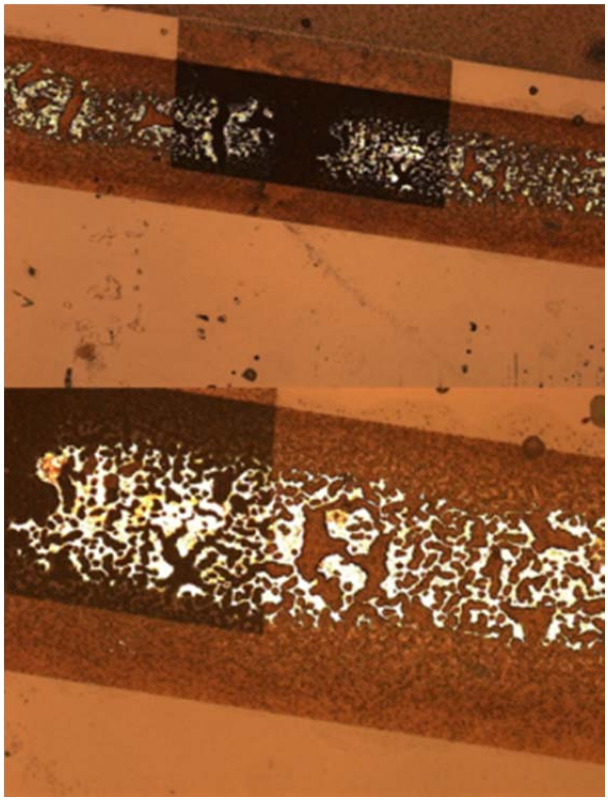

Figure 27: Optical images of Pure Pt paste after 104 hours of heating at 1200°C

Figure 28 (left) shows plots of the real and imaginary parts of a Pt-Ni/Pt-Zr one-port SAW resonator impedance, measured after 850°C 4 hour annealing followed by the six 350°C to 800°C cycles. As can be seen from the data, very stable sensor response was obtained. Figure 28 (right) shows resistance (top) and reactance (bottom) for the a 3.5μm finger width Pt-Ni|Zr one-port SAW resonator obtained at room temperature after 4 hours of anneal at 850°C, 12 hours at 1100°C, and 24 hours at 1100°C thus revealing the device resilience to exposure to 1100 °C for 24 hours.

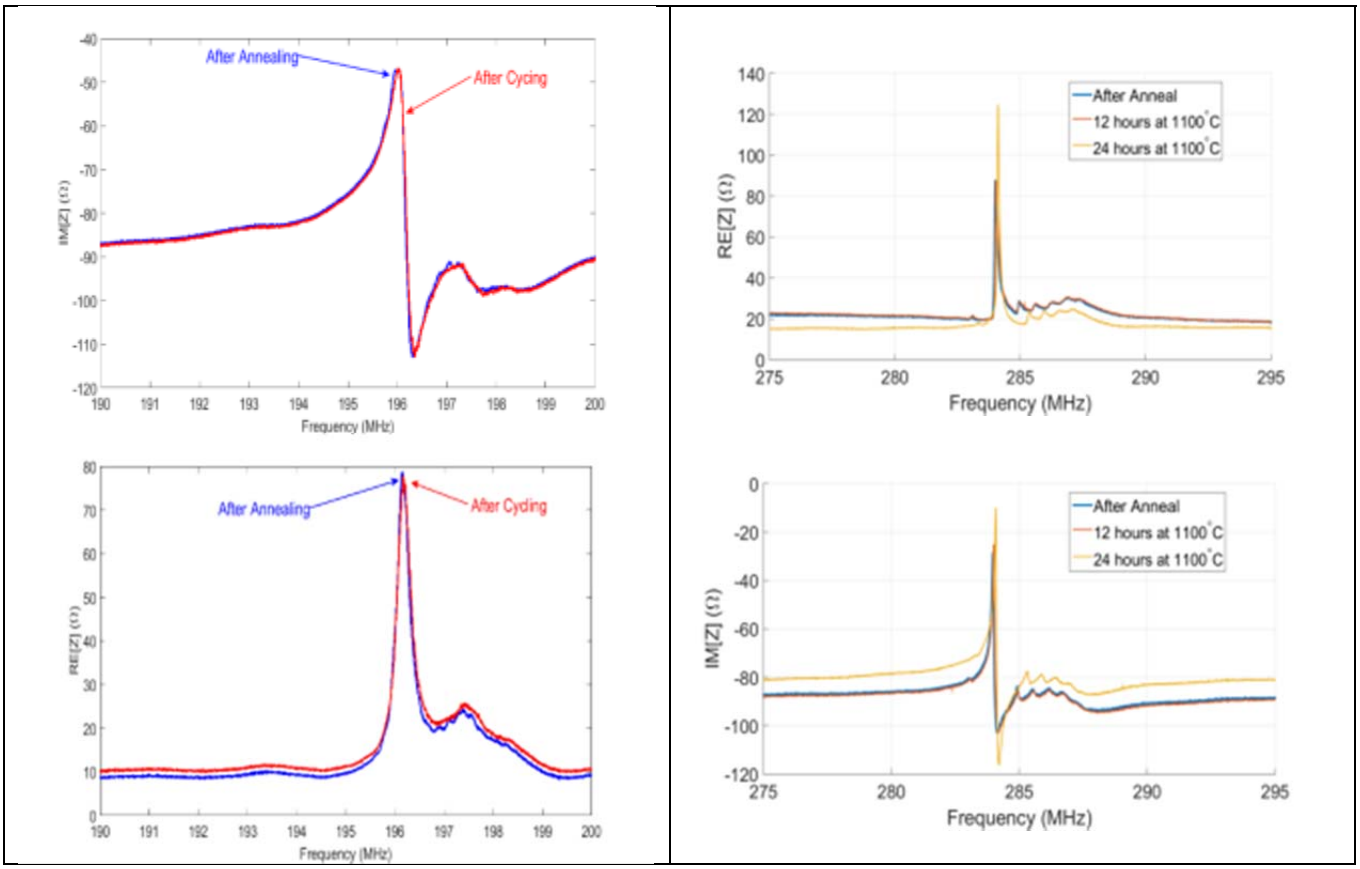

Figure 28: (Left) Resistance (top) and reactance (bottom) for the a 3.5µm finger width Pt-Ni/Pt-Zr one-port SAW resonator measured at room temperature after the 850°C /4hour annealing and after cycling 6 times from 350°C to 800°C. (Right) Resistance (top) and reactance (bottom) for the a 3.5µm finger width Pt-Ni|Zr one-port SAW resonator obtained at room temperature after 4 hours of anneal at 850°C, 12 hours at 1100°C, and 24 hours at 1100°C.

Figure 29 shows the measured resonant frequency vs. time for a Pt-Ni/Pt-Zr one-port SAW resonator, and respective thermocouple temperature over 110 hours stability test, with 56 hours at 1000°C. As shown in the Figure 29, the test was divided into three sections: (1) four cycles from 300°C-1000°C, (2) 48 hours of soaking at 1000°C, and (3) four additional cycles from 300°C-1000°C. The inset of Fig. 4 shows details of the SAW sensor resonator mounted on a high temperature Inconel coaxial cable with the K-type thermocouple used as a reference.

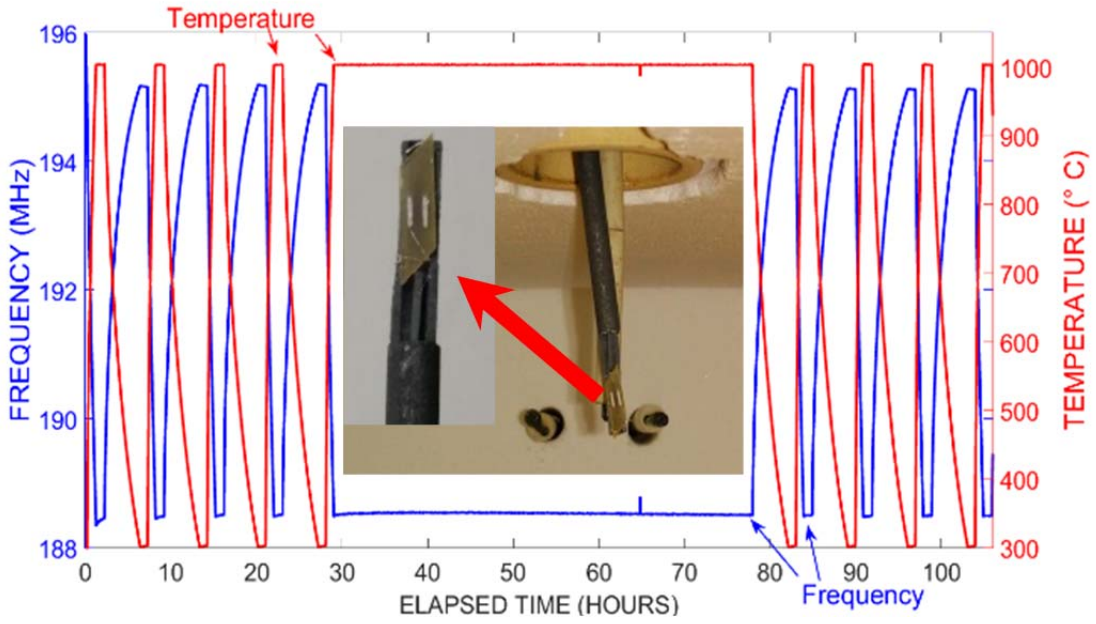

Figure 29: Measured resonant frequency vs. time for a Pt-Ni/Pt-Zr one-port SAW resonator, and respective thermocouple temperature over 110 hours stability test. The inset show the experimental setup, and the details of the one-port LGS SAW resonator and the nearby K-type thermocouple.

The results obtained concerning sensor stability qualifies the high-temperature harsh-environment SAW sensor technology for short-term (tens of hours) operation up to 1100°C, and stable operation at 1000°C for at least several hundreds of hours.

6.2.3 Improved Sensor Fabrication Techniques

Interfacial / Capping Layer Results

The interfacial and capping layer structures have been discussed and justified in Section 6.1.3 of this report, and the structure depicted in Figure 8. In terms of device performance, the relevance of these structures has been verified by the results shown in Table 2 of Section 6.2.2.

Figure 30 (top) shows a SEM backscatter image of a focused ion beam (FIB) cross section of a SAW resonator IDT layered structure, representative of the schematic structure discussed in Figure 8. On top of the LGS substrate, one finds a 50nm interfacial ALD Al_2O_3, followed by the PtRh|HfO_2 electrode of 190 nm, then another 50nm ALD Al_2O_3 as a capping layer, and finally the Zr/Pt/thick paste Pt (approximately 10µm). Note that the structure retains its form after heating at 850°C for 4 hours.

Figure 30 (bottom) shows a SEM image of this same cross section after heating to 1000°C for 4 hours. The device which had this cross section was still operational after heating at 1000°C for 4 hours. The nice layered structure of Figure 30 (top) becomes completely intermingled (Figure 30 bottom) due to the dynamics of the thin-films after exposure to heating at such temperature. The

capping layer appears continuous, but the nanocomposite electrode layer shows extensive phase separation and the interfacial alumina has interdiffused with the LGS substrate, causing voids near the original interface.

Therefore, the structure shown in Figure 8 and Figure 30 was successful in extending the sensor temperature operating range by retarding agglomeration and phase separation, as shown in Table 2, but also start to suffer changes once exposed to enough heat in a certain time period, in the case shown in Figure 30, 1000°C for 4 hours.

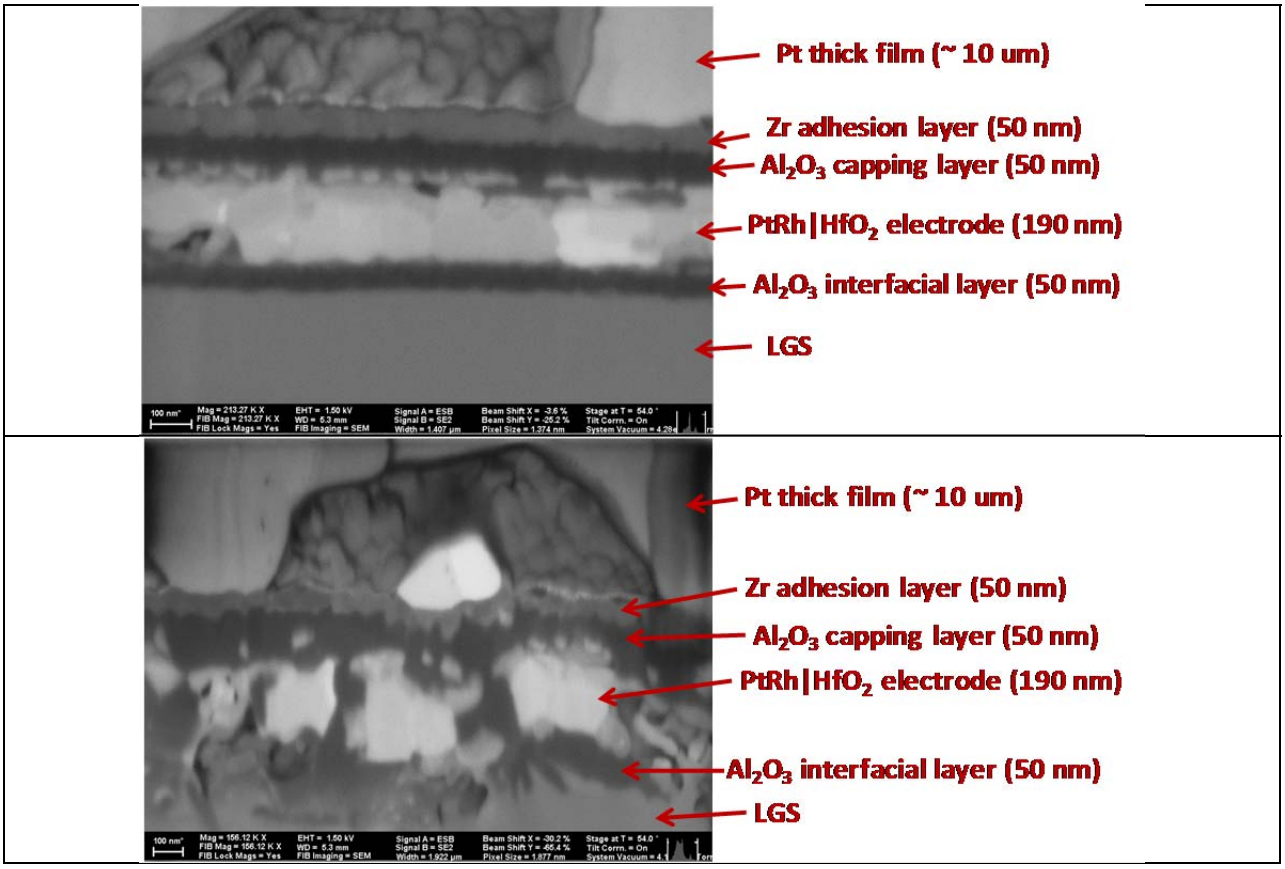

Figure 30: (Top) SEM backscatter image of a focused ion beam (FIB) cross-sectioned SAW resonator bond pad that was heated at 850°C for 4 hrs. (Bottom) SEM backscatter image of a FIB cross-sectioned SAW resonator bond pad that was heated at 1000°C for 4 hrs.

Capacitive Coupling Results

As introduced in Section 6.1.3, the ALD Al_2O_3 insulating layer is used on top of the entire device to isolate the LGS substrate from the environment and to retard the agglomeration of the thin film electrode. The existence of such layer prevents direct bonding to the busbars (contacting pads) of the IDT. In any case, a direct bonding connection between the busbar thin-film Pt-alloy and the one mil Pt wire has been shown to be inadequate at temperatures approaching 1000°C, as mentioned in Section 6.1.3, and also shown in Figure 31. As can be observed from Figure 31, a gradient in the Pt concentration perpendicular to the wire due to diffusion takes place, and larger holes are observable in the film adjacent to the wire where the resultant film composition is Pt-

rich. There is also a noticeable band of film material with the lowest concentration of holes, and this area apparently has the optimal composition of Pt. Far away from the wire bond, the film has the as-deposited concentration of Pt and smaller holes compared to the Pt-rich region adjacent to the wire. This Pt diffusion and dewetting near the Pt bond wire accelerates the electrode deterioration. This degradation compromises the wire bond reliability and the device stability at high-temperature, ultimately leading to contact failure.

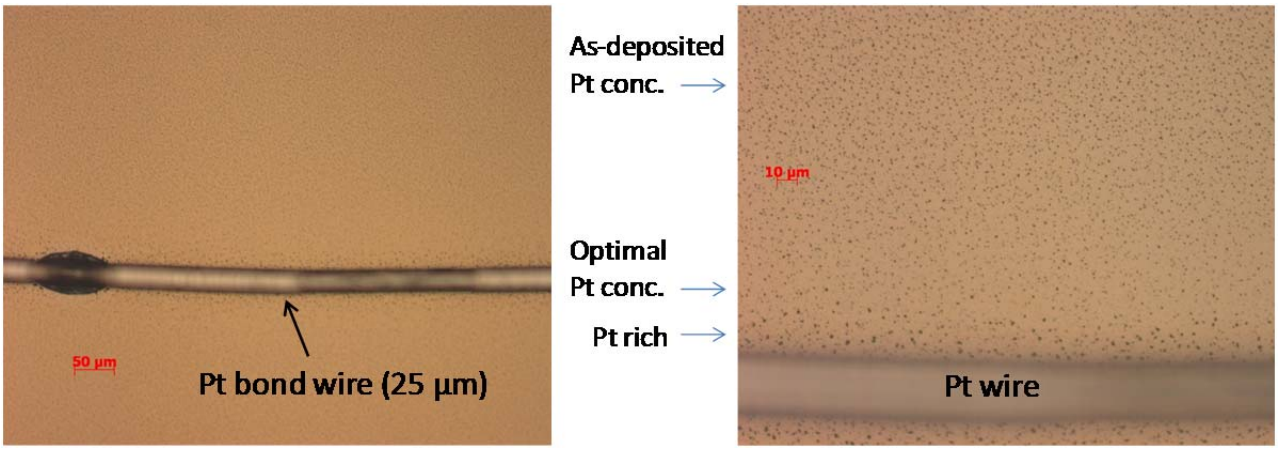

Figure 31: Optical microscopy of Pt bond wire attached to PtRh/HfO2 film after heating at 1000°C for 5 hrs.

The capacitive coupling technique, implemented under this project, becomes a necessity for high temperature access of the IDTs of the SAW sensor. Figure 32 shows an implementation of a capacitive coupled SAW device with the deposited thick Pt paste. All the devices for the measured responses in Table 2 utilized this technique.

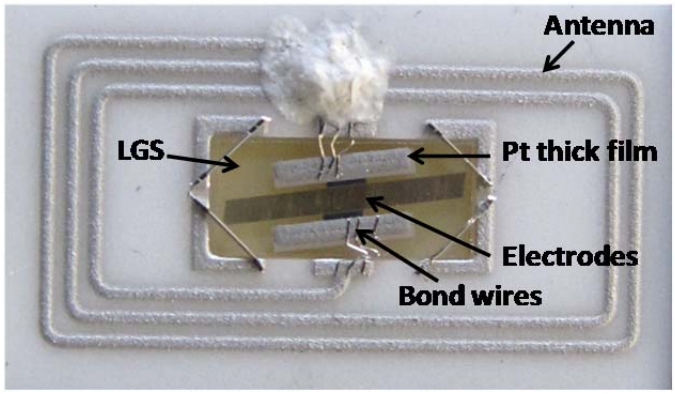

Figure 32: Optical micrograph of a SAW device bonded to an antenna and employing the capacitive coupling technique through thick Pt paste bonding contacts.

6.2.4 In-house Fabricated HT Furnace

The high temperature positioning furnace was successfully designed, fabricated, and implemented for tests which included the development the LGS wireless SAW technology for power plant applications where the flexibility in applying wireless sensors to moving parts is of major importance. The furnace wall are made of thermo-insulated materials (Figure 33 top left), not metal, thus allowing wireless interrogation from outside, differently from a metal box, which operates as a Faraday cage, shielding the external wireless signal to and from the sensor (Figure 33 top right). The furnace counts with an automated positioning system, which allows the placement of the sensor and antenna inside the chamber at different locations (Figure 33 bottom).

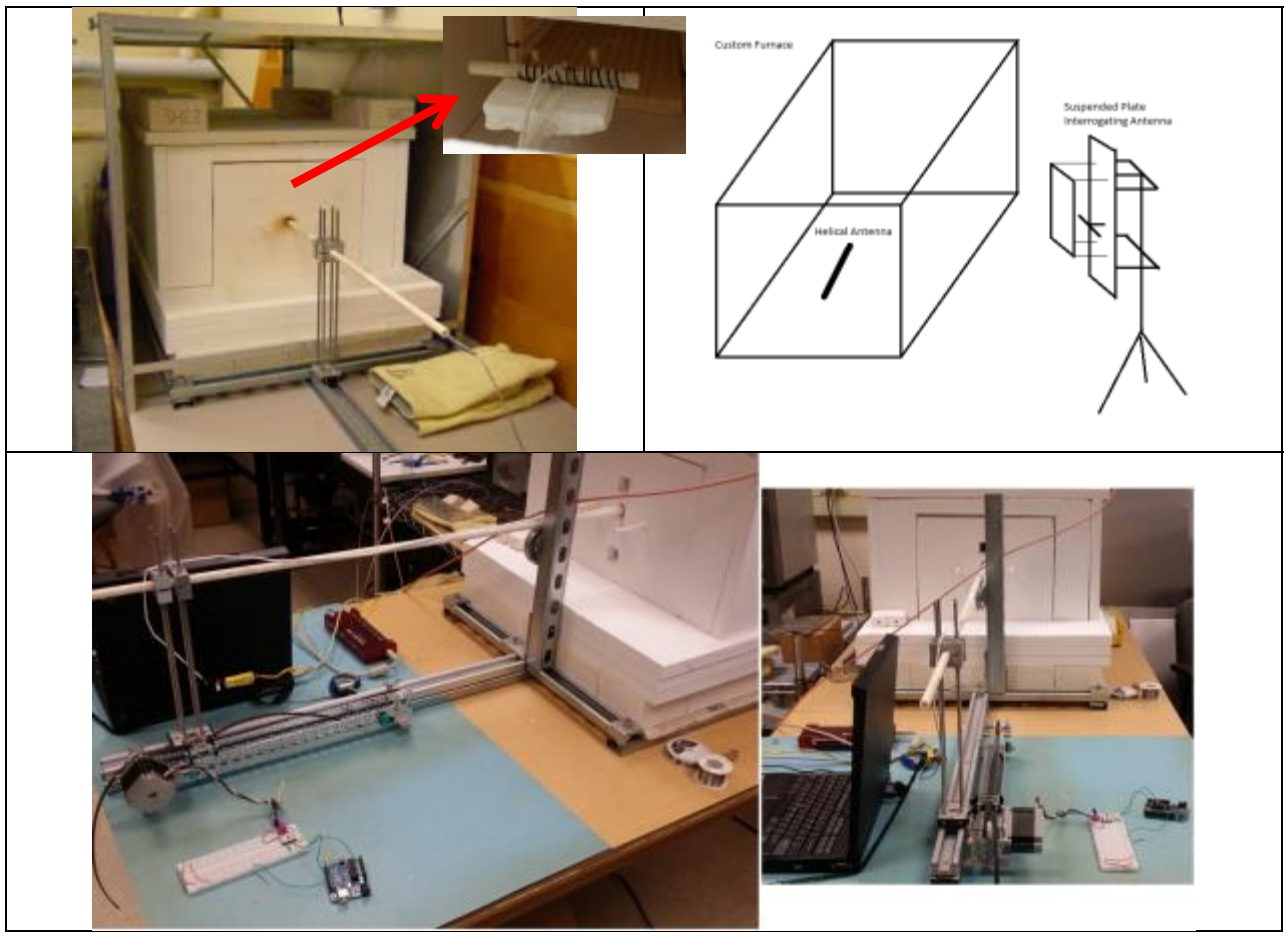

Figure 33: Wireless Testing Furnace (also referred to as Position Furnace). Capable of operating up to 1200 °C; Automated sensor positioning system

Figure 34 shows the SAW resonator frequency as a function of the position into the furnace. The negative and positive values in the coordinate axis indicate movement towards the center of the furnace (hottest region) and back to the door of the furnace (coolest region).

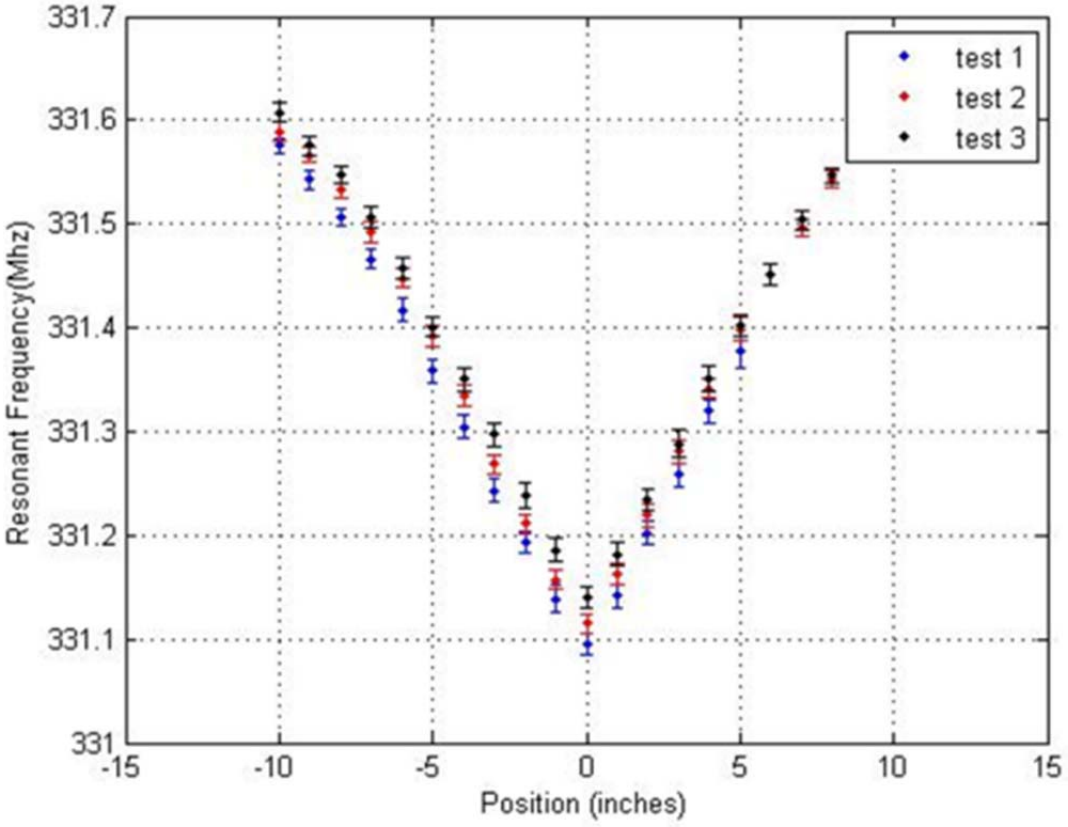

Figure 34: Frequency as a function of distance; the zero position takes place at the center of the furnace. The negative and positive values in the coordinate axis indicate movement towards the center of the furnace (hottest region) and back to the door of the furnace (coolest region).

The furnace was calibrated by using K-type thermocouples in close proximity to the SAW sensor. Figure 35 shows the SAW sensor calibration curve utilizing the referred thermocouples. The standard deviation of SAW frequency is shown as the horizontal bars whereas the vertical bars considers the standard deviation of the thermocouple data.

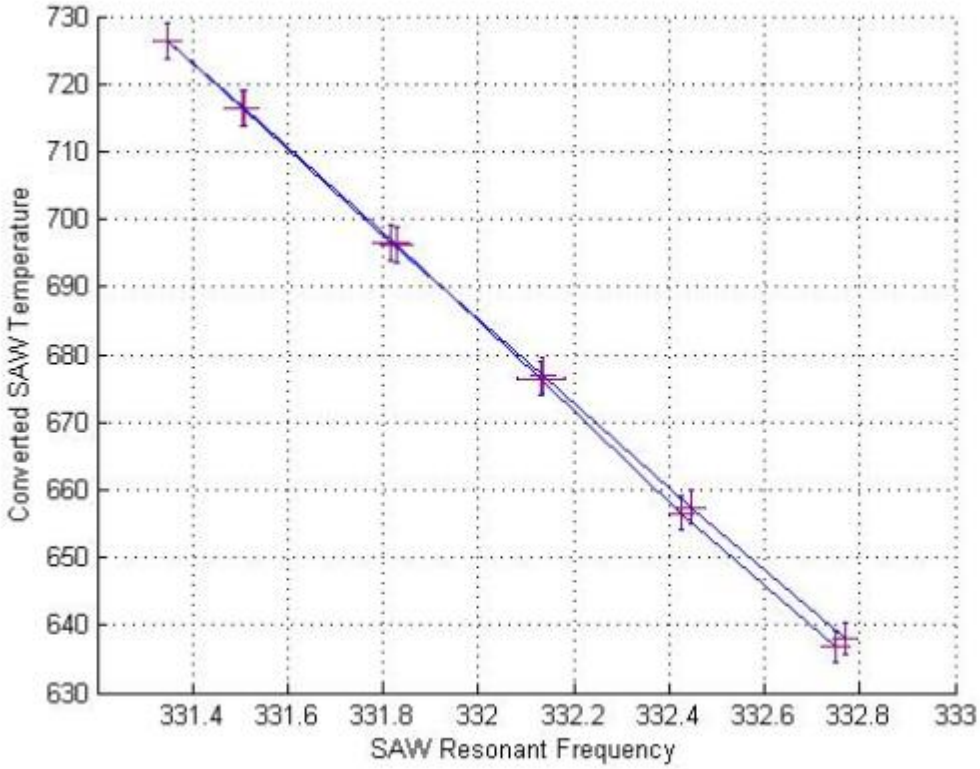

Figure 35: Experimental calibration curve established for the sensor. Linear curve fitting was applied to this data. It should be noted the reference thermocouple used has an error rating of 0.75°C.

6.2.5 Technology Transition

Tests at NETL

Two tests have been performed at the NETL / Combustion Science Division Aerothermal facility, Morgantown, WV, as introduced in Section 6.1.5. The first tested aimed at learning about the test system and identifying issues with materials and packaging involved in the fabrication and mounting of SAW sensors, sensor antennas, and interrogating antennas. The second test targeted operational conditions of several sensors embedded and on the surface of two similar new coupons, interrogated wireless or wired, and compared with thermocouples, mounted in the vicinity of the SAW sensors.

Test of Materials

Figure 36 is a picture with the details of several of the structures tests in a coupon kindly furnished by the NETL. The materials involved in the test included LGS substrate with SAW resonators, gold plated antennas on LGS and on alumina, and an Inconel loop antenna. The devices were held by 4 mil Pt wires or steel shim stock spot welded to the coupon.

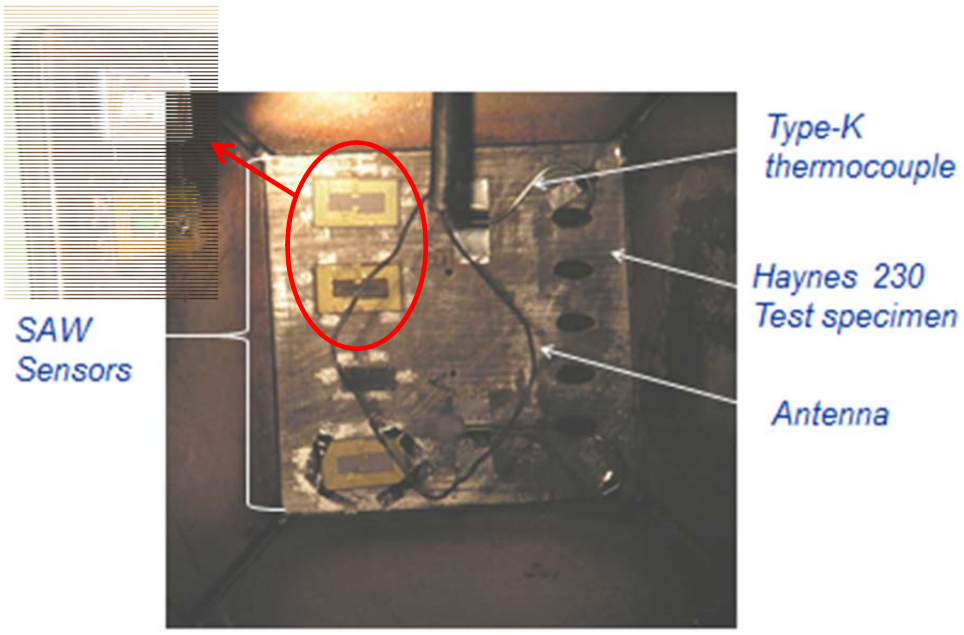

Figure 36: Test coupon and interrogation installed in test rig (photo courtesy of NETL).

Figure 37 shows the coupon previous described under test in the gas combustor chamber of the NETL Aerothermal Facility (view from the inner viewport window). As can be noted from the color intensity of the parts, the coaxial cable that served as support for the loop antenna is at much higher temperature (about 1100°C) than the coupon itself (about 750°C). The loop was completely burnt in this case, and one of the chips flew away, blown by the flowing gas in the chamber (see Figure 10). This finding allowed the UMaine/Environetix team to improve the packaging and elaborate the second test which results are reported next.

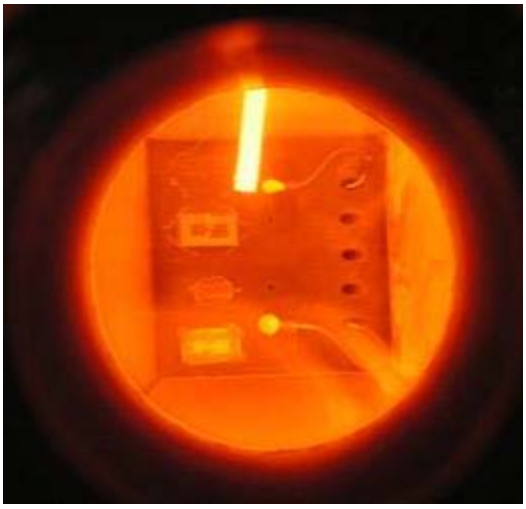

Figure 37: Coupon under test in the gas combustor chamber of the NETL Aerothermal Facility. View from the inner viewport window.

Test of Wired and Wireless Sensor Coupon

Eight SAW temperature sensors were mounted in 2 test coupons, as detailed in Figure 38. A wireless sensor and a wired SAW sensor were secured into milled pockets by spot-welding 1 mil thick Inconel shim stock over two ends. Reference thermocouples were also attached adjacent to the sensors with Inconel shim. Two pieces of 0.5 mm thick alumina, shown in Figure 38, act as caps over holes drilled through the coupon. These two cylindrical pockets housed two additional probe style SAW sensors that were inserted into the coupon from the back.

The probe assemblies were fabricated by milling away part of a high temperature coaxial cable and partially embedding a SAW device into epoxy. A reference thermocouple was attached to the cable jacket by spot-welded Inconel shims. The wireless sensor consists of a Pt thick film receiving antenna printed on a 0.5 mm thick alumina substrate connected to the SAW device printed on a LGS substrate. The SAW device is held in a laser machined pocket in the alumina antenna by four Pt wires spot-welded over the corners of the LGS substrate (see Figure 38).

A wireless interrogating antenna was assembled and Hastelloy fixture with an alumina cover, as shown in Figure 39, considering that the antenna is exposed to the gas flow at much higher temperature (~1100°C) than the surface of the coupon (~750°C). The alumina cover was placed over the antenna holder to protect the electrical connections from turbulent air forces.

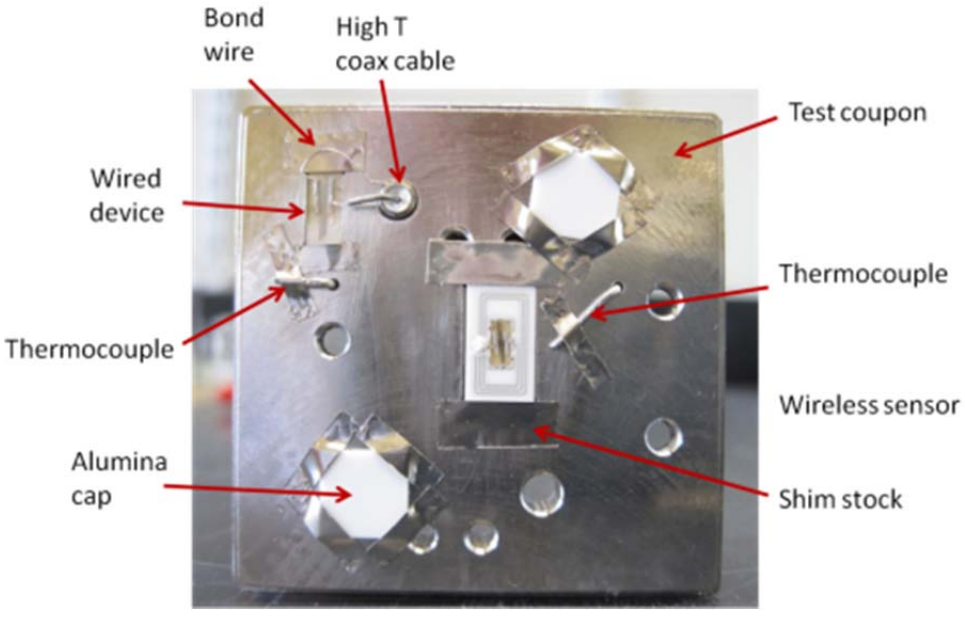

Figure 38: Test zone face of instrumented NETL coupon.

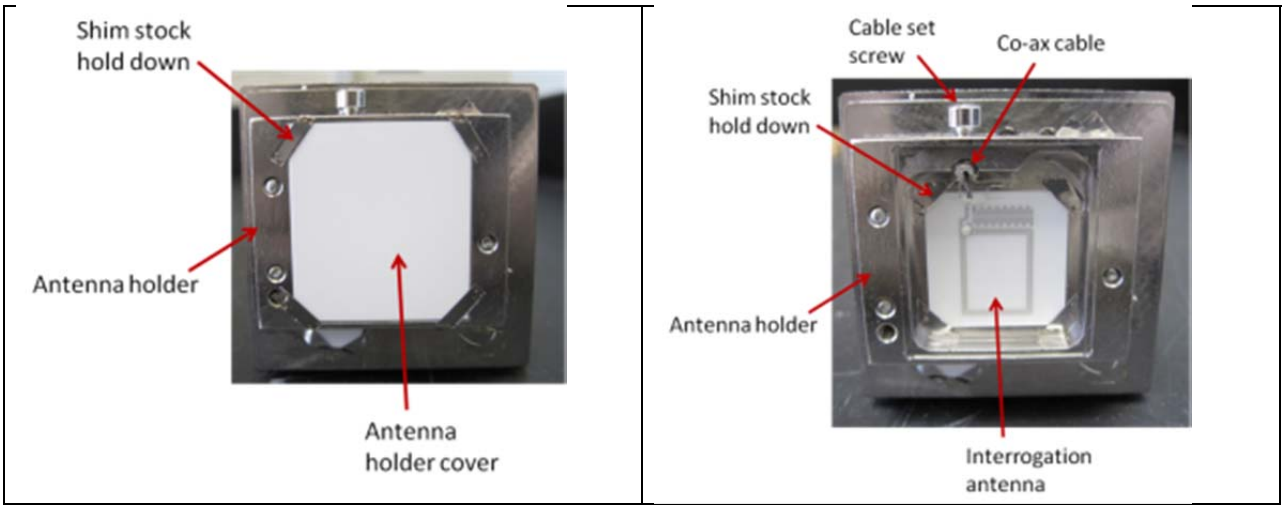

Figure 39: (Left) Covered and opened (right) interrogation antenna assembly for the NETL coupon.

Prior to the tests at the NETL / Combustion Science Division Aerothermal, Environetix conducted furnace testing of all SAW sensors up to 850°C to verify the stability of the devices used for the NETL test, and to generate appropriate calibration curves to convert resonance frequency measurements to temperature in real-time.

The two coupons were mounted and tested one at a time at the NETL Aerothermal combustor chamber for a full day of test each. Mounting each coupon took a day, and testing each one of them took another day. The objectives of the testing were to:

1) Verify high-temperature sensor operation in the test rig;
2) Compare sensor responses with and without a protective Al_2O_3 capping layer; and
3) Compare SAW temperature sensor measurements to witness thermocouples.

The testing protocol involved stepping upwards in exhaust temperature from 650°C (1200°F) to a maximum 1150°C (2100°F). The temperature was held constant for 1h for each intermediate step. The temperature readouts of all SAW sensors and thermocouples are shown in Figure 40.

During assembly of Coupon 1 on the NETL testing fixture, it was noted that the steel thermocouple guide tubing within the plenum placed severe constraints on the available space for the UMaine/Environetix thermocouple wires. As a result, several of the witness thermocouples were crimped, and 2 of the 4 thermocouples, in particular those thermocouples attached to the probe style sensors, had readings that agreed more closely with the plenum temperature than with the temperature at the coupon. This problem was remedied for the 2nd day of testing by cutting off the thermocouple guides.

The wireless sensor measurement agreed with surface thermocouple measurement up to a surface temperature of approximately 760°C. The wired embedded probe devices, and surface-mounted 3.5µm device were tracked for the duration of the test. Although thermocouple witnesses for the wired probes were damaged, these sensors all demonstrated agreement with the expected coupon

temperature, which was between the measured surface and plenum temperatures. The surface mounted thermocouple adjacent to the 3.5µm device indicated a temperature approximately 50°C above that indicated by the SAW sensor.

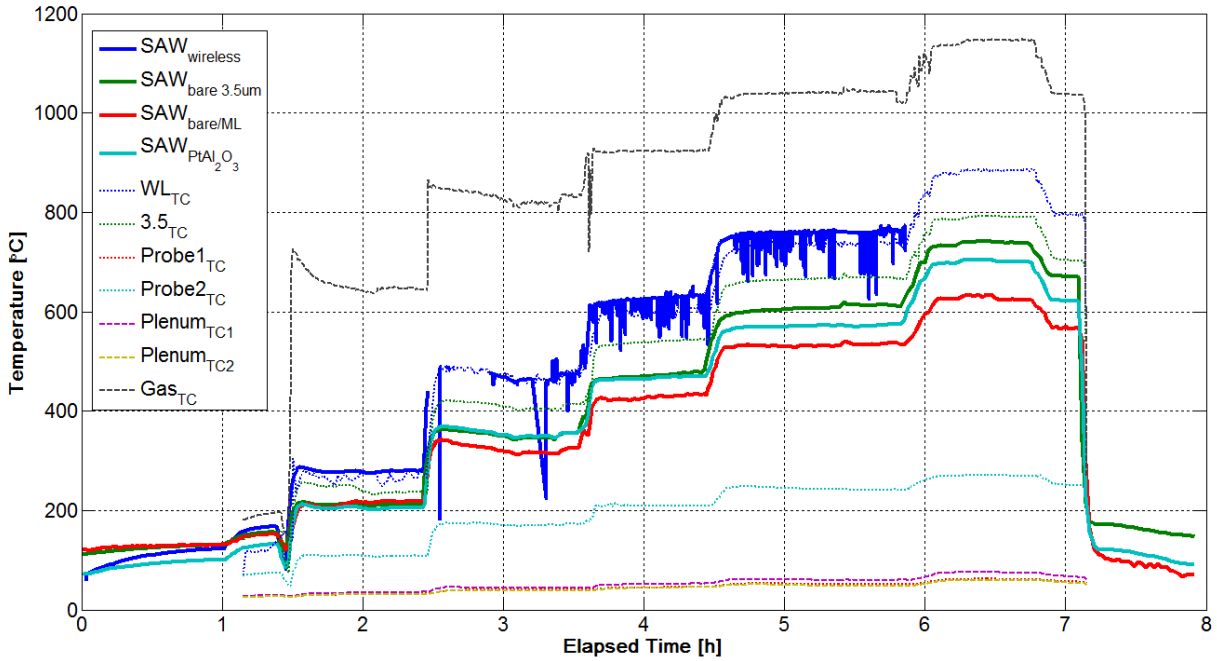

Figure 40: Temperature readout from all sensors on one of the coupons under test. Solid lines indicate SAW sensors. Dotted lines indicate UMaine/Environetix witness thermocouples mounted on the coupon, including damaged thermocouples. Dashed lines indicate NETL thermocouples.

Resonance frequency as a function of temperature F(T) was plotted for each device, alongside the original calibration curves. The results from Coupon 1 are shown in Figure 41 (Coupon 2 results were similar). The F(T) curve shapes for all devices were similar to the prior calibrations. Other than a more significant frequency drift observed on one of the devices, the calibration curves were very similar prior and post-test. Differences were credited to two causes: (i) surface contamination and deterioration of the devices directly exposed to the eight hour test (see Figure 42); and (ii) incomplete annealing of the devices mounted, a process that has been improved after these tests were performed.

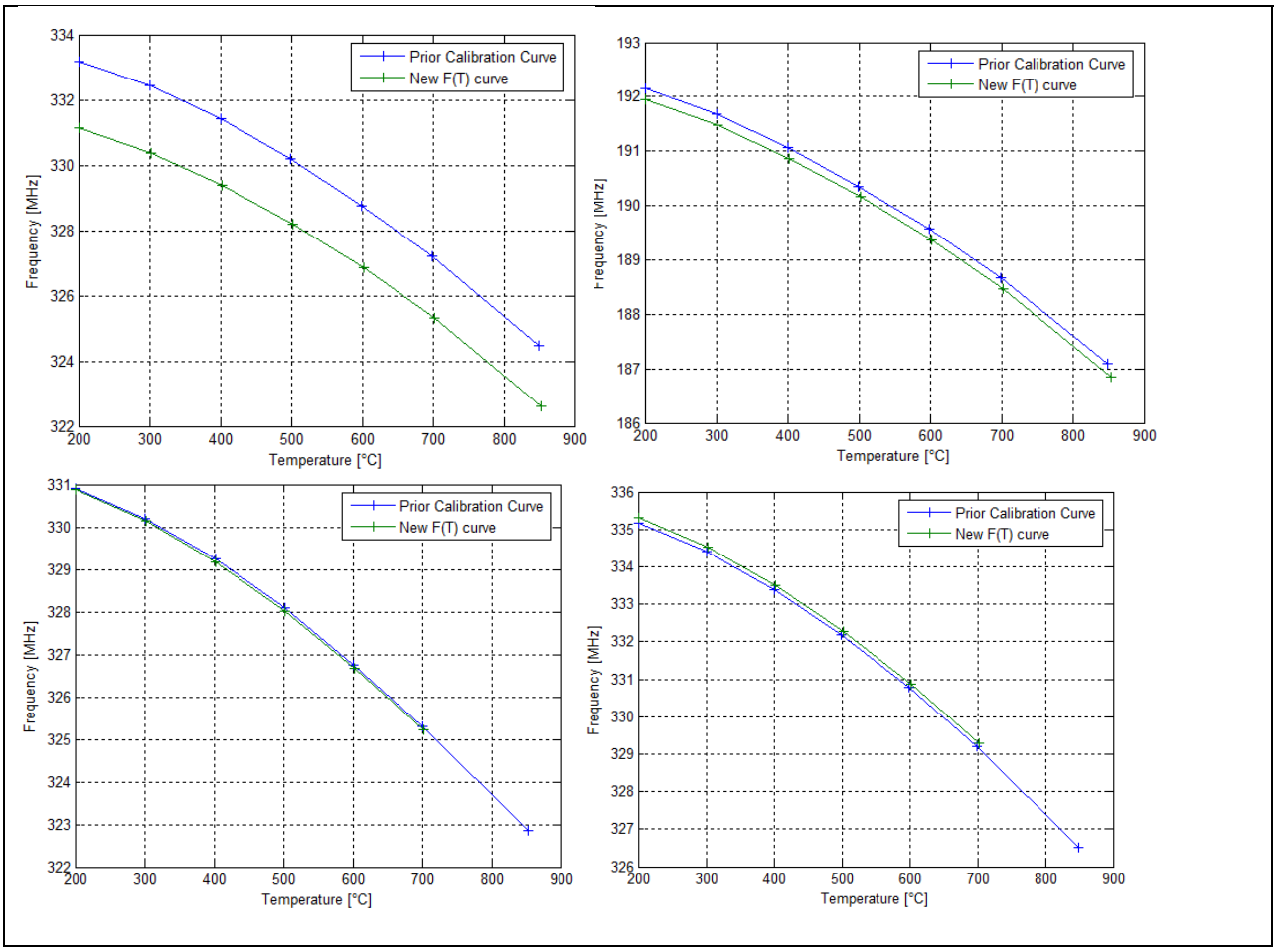

Figure 41: Resonance frequency as a function of Temperature plots for Coupon 1 devices. Top left: Wireless; Top right: wired surface; Bottom left: Probe 1; Bottom right: Probe 2.

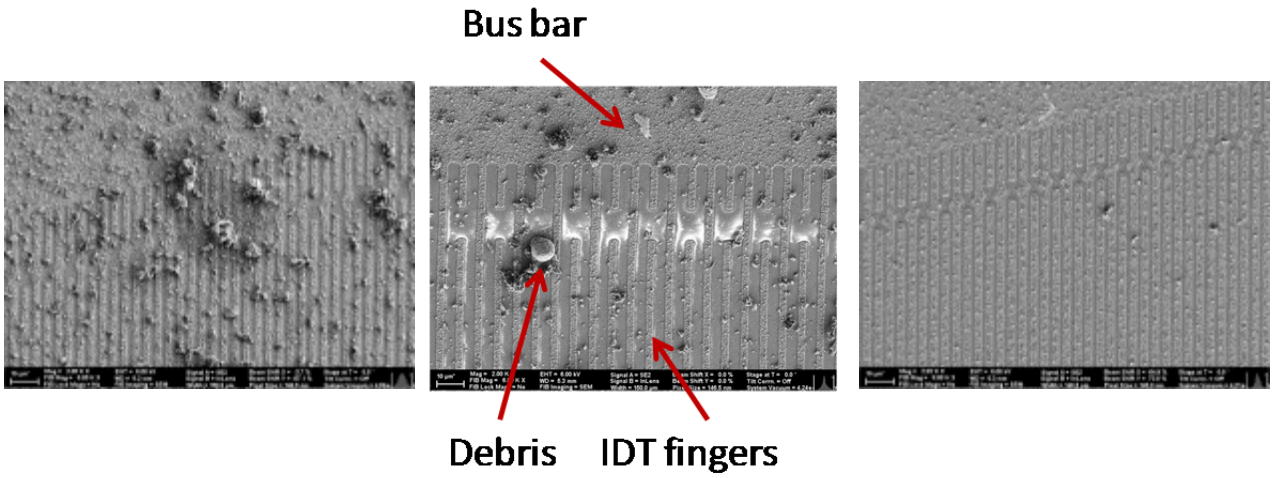

Figure 42: SEM of wireless device (left), wired surface device (middle), and probe 2 device (right). The first two were exposed to the environment, while the third was protected in the coupon holes.

The results obtained after the tests described above with the two coupons during a week of work at the NETL Aerothermal facility showed that the packaging and mounting techniques were adequate, and that the sensors were stable and resilient enough, in particular if the surface is not directly exposed to the flux of gas and particulates, to perform high-temperature harsh-environment monitoring functions. These results granted the next phase of tests at the PERC power plant environment, which is described in the next section.

Tests at PERC

Starting in the first quarter of 2014 until the end of this project in December of 2016, the Environetix/UMaine team tested materials, SAW sensors, antennas, and wireless SAW sensor arrays in the Combustion Chamber, the Economizer Section, and in the last session of the boilers of the PERC power plant. Session 6.1.5 of this report introduced the methods used for testing the developed technology in the PERC power plant environment. In this section, the results are presented and major outcomes discussed.

Material Tests on the Combustion Chamber

Figure 43 (left) shows a schematic diagram from the PERC power plant, repeated from Figure 13 for clarity and convenience, indicating the position of some of the K-type thermocouples encased in Hastaloy fixtures (Figure 43 top right) present in the plant. Also shown in Figure 43 bottom right is the result of exposing the thermocouple Hastaloy fixture to the PERC power plant harsh-environment for a few months. Evidently, this requires constant maintenance, since the erosion and corrosion of the thermocouple casing exposes the device, leading to its destruction. Another disadvantage of the thermocouple is the wiring required to access the device, which must be routed throughout the power plant.

Environetix/UMaine team tested different materials aiming at the construction and packaging of the wireless SAW sensor array. A 36” Inconel test fixture, Figure 44 (top-left), was fabricated and used as the support rod for a 1” by 3” Inconel plate (Figure 44 middle-left) onto which material test specimens were mounted (Figure 44 bottom-left). The fixture temporarily replaced the existing combustion chamber thermocouple shown in Figure 43 right. Figure 44 right, shows the overall test structure after 10 days exposed to the corrosive environment in the PERC power plant. Figure 44 bottom-left shows several pieces of selected harsh environment material candidates mounted on the plate, namely: sapphire, LGS, yttria-stabilized zirconia (YSZ), alumina, ceramic epoxy, Inconel, NiCr and graphite. Figure 44 bottom-right shows these pieces after the 10 day exposure to the environment and removal from the plate.

As can be seen from Figure 44, a thick layer of hardened ash is deposited on the test fixture during power plant operation, completely covering all test materials. After removing the fixture from PERC, the ash was chipped off to allow for inspection of the fixture and the materials. It was found that the Inconel was significantly corroded during the test and the nickel shim stock holding the test specimens in place was completely eroded away. For this reason some of the

samples were not found after removing the ash. The materials shown in Figure 44 bottom-right are: alumina, YSZ, and graphite. Inspection revealed that their surfaces did not display significant wear or damage, and thus could be selected for usage in sensor packaging and fabrication. Alumina was selected as the primary sensor packaging material for the first wireless sensor array fabricated and described next, since it is relatively low-cost and more readily available when compared to the other candidate materials tested.

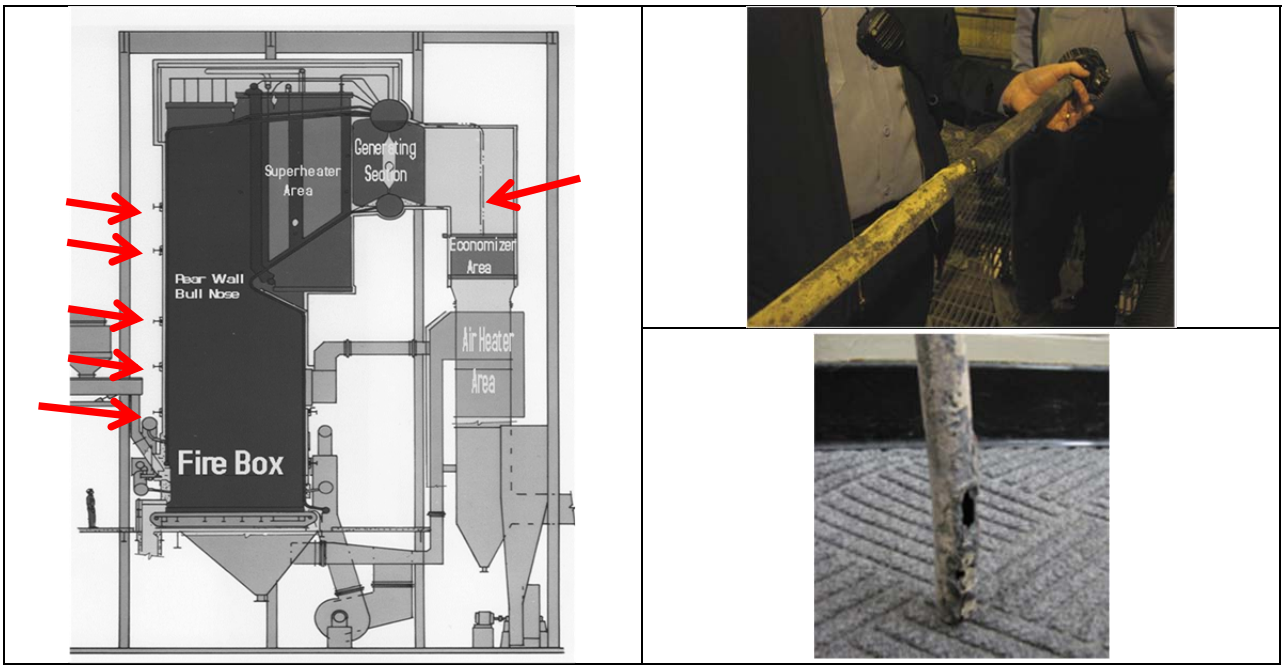

Figure 43: Left: diagram of PERC power plant. Top right: thermocouple Hastalloy fixture from power plant structure. Bottom right: same structure after removal during maintenance.

Figure 44: <u>Top left and right</u>: Inconel fixture, consisting of rod and 1"x3" plate for material testing, before and after exposure to the power plant environment for 10 days. <u>Middle left and right</u>: Inconel test plate before (left) and after (right) exposure to the power plant environment. <u>Bottom left and right</u>: the same Inconel test plate instrumented with different materials, before (left) and after (right) exposure to the power plant environment for 10 days.

Economizer

The array with six wireless SAW sensors fabricated and mounted was depicted in Figure 13. The figure also shows the details of the SAW sensor array system, which counted with 6 sensors, each connected to its own dipole antenna protected by an outside alumina casing, and an interrogating monopole antenna in the center of the structure, also protected by an alumina casing.

Figure 45 shows the labeling used to identify each of the six sensors in the wireless sensor array and the final mounted panel, which was mounted in the Economizer point of access, as shown in Figure 46. Each antenna in the array was tuned for operation with its respective SAW sensor, in the 280-340MHz operational range of the array, as indicated in the caption of Figure 45. The temperature values of the calibrated SAW sensors were compared to the temperature of the power plant thermocouple pointed in Figure 46 (left). The mentioned thermocouple was a few meters away from the array, and thus its temperature was used as a reference, not as a true value for the sensors.

Figure 47 shows the status of the panel after operation for about six weeks. The material deposited as a result of burning wasted material did not degrade any of the external packaging material, as observed after cleaning the structure.

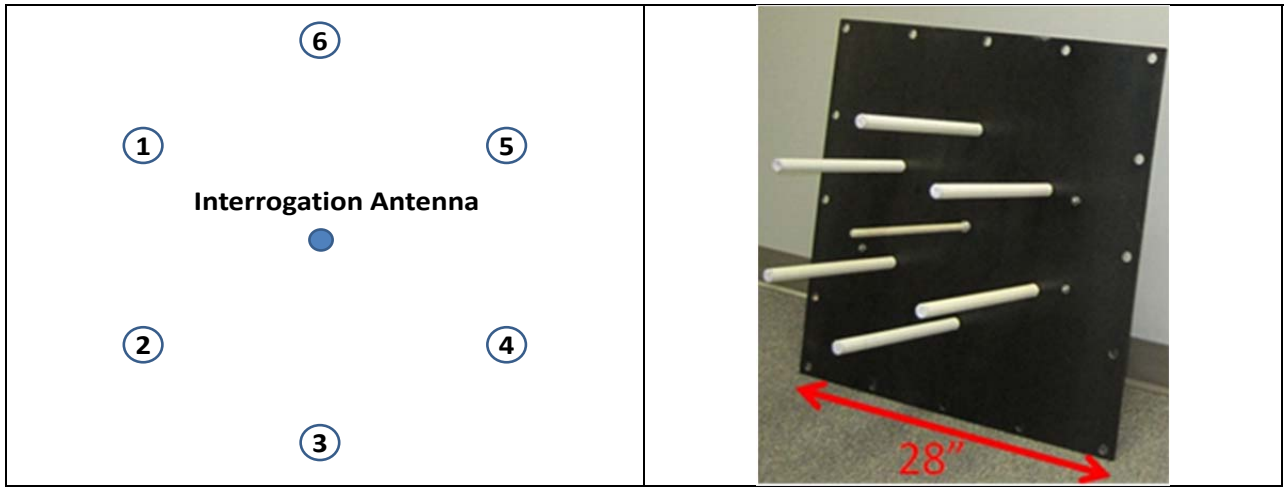

Figure 45: Left: relative location of the interrogation antenna and each wireless sensor with respective antenna in the wireless sensor array; from Sensor 1 to Sensor 6, respective operating frequencies: 281 MHz; 291 MHz; 301 MHz; 313 MHz, 321 MHz; 337 MHz. Right: final mounted panel.

Figure 46: Left: sensor array panel installed at PERC. Right: Environetix engineer performing wireless interrogation tests with the six sensor array panel.

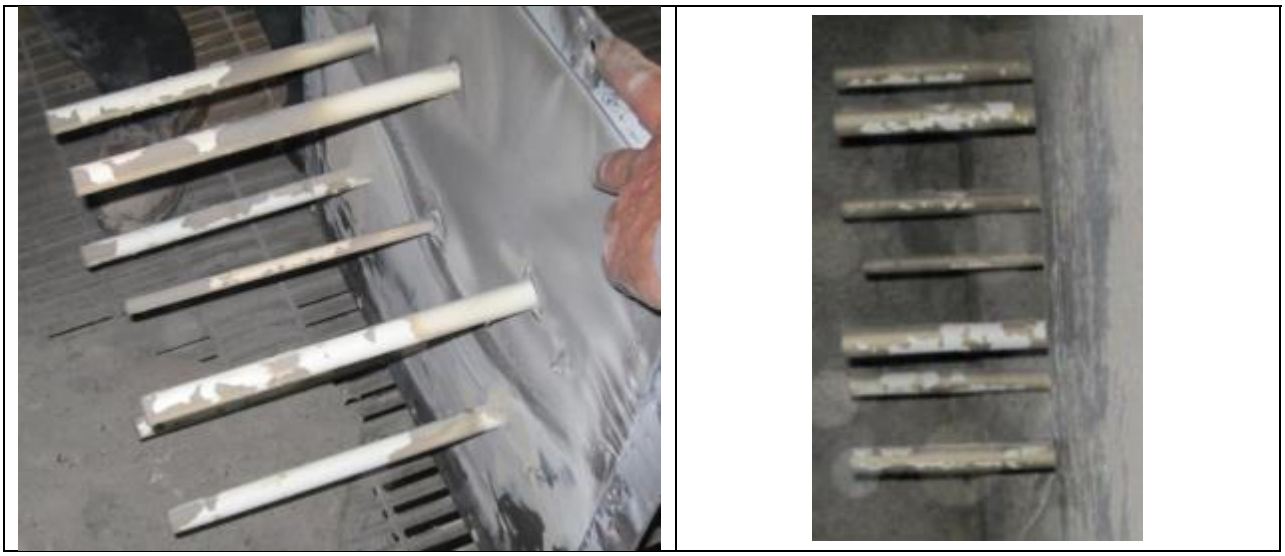

Figure 47: Panel inspection after six weeks operation and plant shut-down.

Table 3 shows that the difference between the temperature reading of K-type thermocouple located a few meters away and the average of the six wireless interrogated SAW sensors is within one percent for each measuring instance. Given the significant airflow and cooling that occurs in the PERC economizer area a discrepancy is expected between the wireless sensors and the PERC thermocouple. Moreover, no clear sign of external packaging degradation was found in the structure.

Figure 48 plots the multiple readings for the five measuring instances shown in Table 3. From this test it was found out that the SAW device was not affected by the power plant operation due to the protection offered by the packaging used. However, the NiCr antenna conductors connected to the sensors suffered severe oxidation, which led to the attenuation of the signal amplitude with time, as can be seen in Figure 48. This finding led to the replacement of the NiCr with more resilient Inconel wire. Several other packaging improvements have been performed throughout almost two years of testing with this fixture.

The array of six LGS SAW sensors was wireless interrogated throughout a period of about two years in the corrosive and erosive PERC power plant environment, which burns municipal solid waste. During the test period, different packaging techniques were explored, but most importantly, the wireless SAW sensors developed showed their resilience for the targeted measurement in such hostile environment, and their consistency in reading compared to the available thermocouple (within 1% for each measurement instance), and later with thermocouples inserted in the fixture by Environetix.

The reliable sensor operation over extended periods of time and the positive results obtained with the wireless SAW sensor array structure encouraged the continuation of the technology transfer to other applications within the power plant. In the next section, the effort to place a wireless SAW sensor array on the exposed part of the boilers at the PERC power plant is discussed.

Table 3: Temperature measured by each sensor in the wireless sensor array and the PERC thermocouple

Date	Sensor 1 (°F)	Sensor 2 (°F)	Sensor 3 (°F)	Sensor 4 (°F)	Sensor 5 (°F)	Sensor 6 (°F)	PERC TC(°F)
Week 1	684	673	684	679	680	696	688
Week 2	694	684	695	670	688	706	693
Week 3	706	691	702	705	688	711	698
Week 4	712	689	701	702	671	711	691
Week 5	763	737	741	748	750	728	738

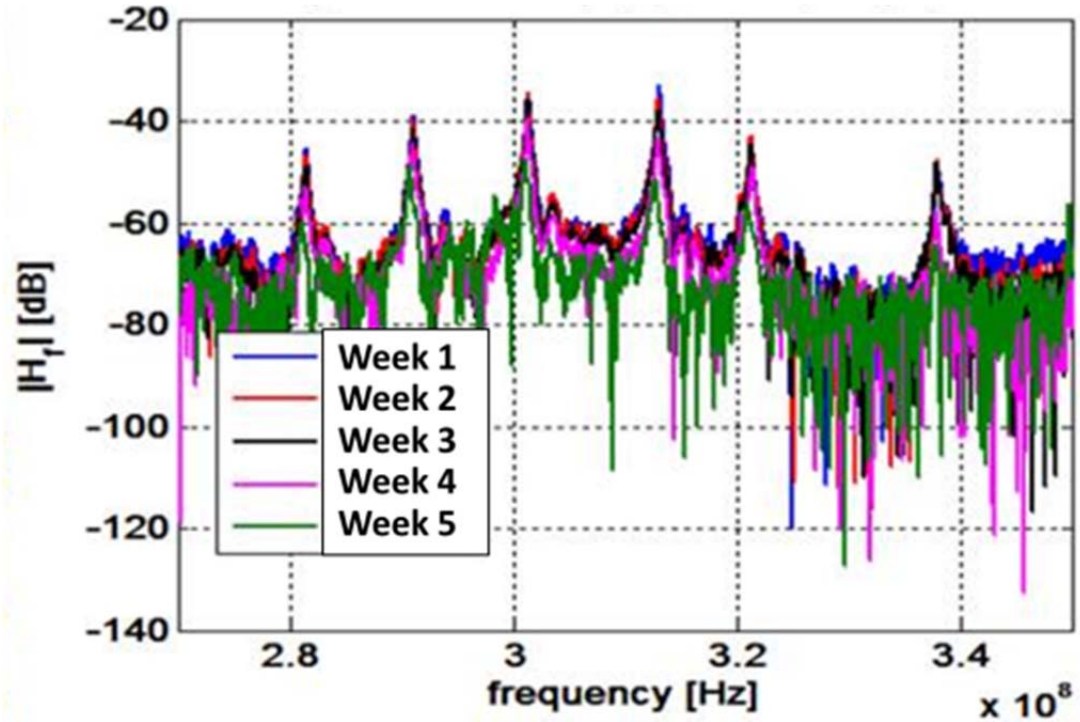

Figure 48: Processed data showing unique resonance frequency peaks for the six wireless sensors interrogated as indicated in Table 3.

Boiler Tubes

As introduced in Section 6.1.5, *Methods for Testing in Power Plant Environment*, the target of this effort was to transfer the developed wireless SAW high-temperature harsh-environment technology to applications within the power plant, where the introduction of the new technology can have a significant impact.

After conversation with PERC personnel, it was identified that monitoring the temperatures of the boiler tubes in different locations and with time, will allow the continuous monitoring of clogging along the boiler tubes. Clogs in the superheaters and boilers through slagging, restricts the gas flow, diminishes the heat exchange, and reduce the power plant efficiency. In addition the soot accumulation in the tubes can lead to fires, which inevitably damage them, reducing the operational life of the equipment, and posing operational risks. Soot blower are used to dislodge the soot, but now continuous or precise information exists in most plants to identify when and where is more important to remove the soot.

Figure 14 in Section 6.1.5, showed the deployment of an array of sensors by Environetix/UMaine on the back part of the boiler section. This location was used due to the existing access from the economizer section, which allowed the placement of the interrogation antenna, next to the location where the old array was installed (see Figure 49), thus reducing the interference with the power plant operation. The installation was done during the scheduled yearly maintenance of the tubes, when the power plant shuts down for about two weeks. The window to install the equipment was only two days.

Figure 50 shows a view from inside the economizer chamber (at another angle from the one shown in Figure 14), revealing the interrogation antenna fixture, which is 90° from the boiler pipes, and the positioning of several of the sensor array elements mounted to the boiler tubes.

Figure 49: The new door location indicated in the picture served the purpose of housing the interrogating antenna for the boiler sensor array.

Figure 50: Interrogation antenna and relative positioning with respect to boiler tubes. Some of the wireless SAW sensor array elements mounted on the boiler tubes are also visible in the figure.

Figure 51 left shows a packaged wireless sensor unit under laboratory testing and prior to mounting in the boiler tube. Figure 51 right shows the measured signal processed sensor response. The sensor array element was wirelessly interrogated in the lab from a distance of over 3 meters.

Figure 52 shows a typical sensor response for an array element mounted in the PERC boiler tube. Table 4 shows wireless temperature measurements from two of the installed sensors at the boiler under operation. The PERC thermocouple temperature (TC temp) is also included in Table 4 for reference only since it close to the wall of the economizer, and thus far away from the boiler tubes (see Figure 46). One can note that the temperature on the wall of the economizer is significantly lower than the temperature at the boiler tubes. Also, after two weeks the thermocouple on the economizer wall measured a temperature variation of only 5°F, whereas the two wirelessly interrogated sensors indicate a variation of about 48°F between them.

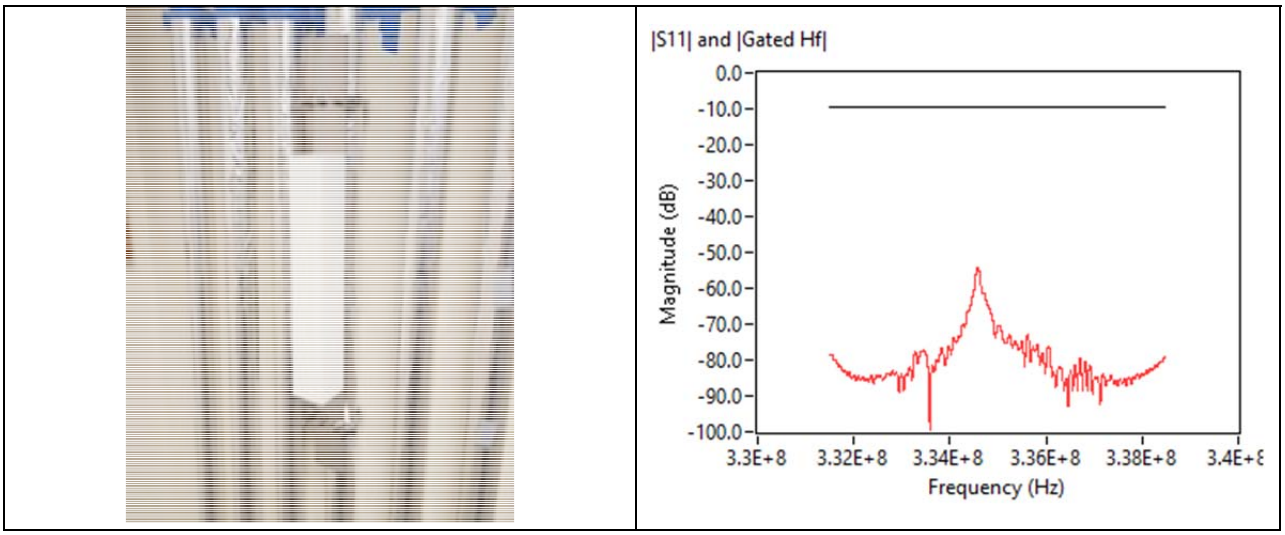

Figure 51: (Left) Packaged wireless sensor unit under laboratory testing and prior to mounting in the boiler tube. (Right) Signal processed sensor response wireless interrogated at a distance of over 3 meters.

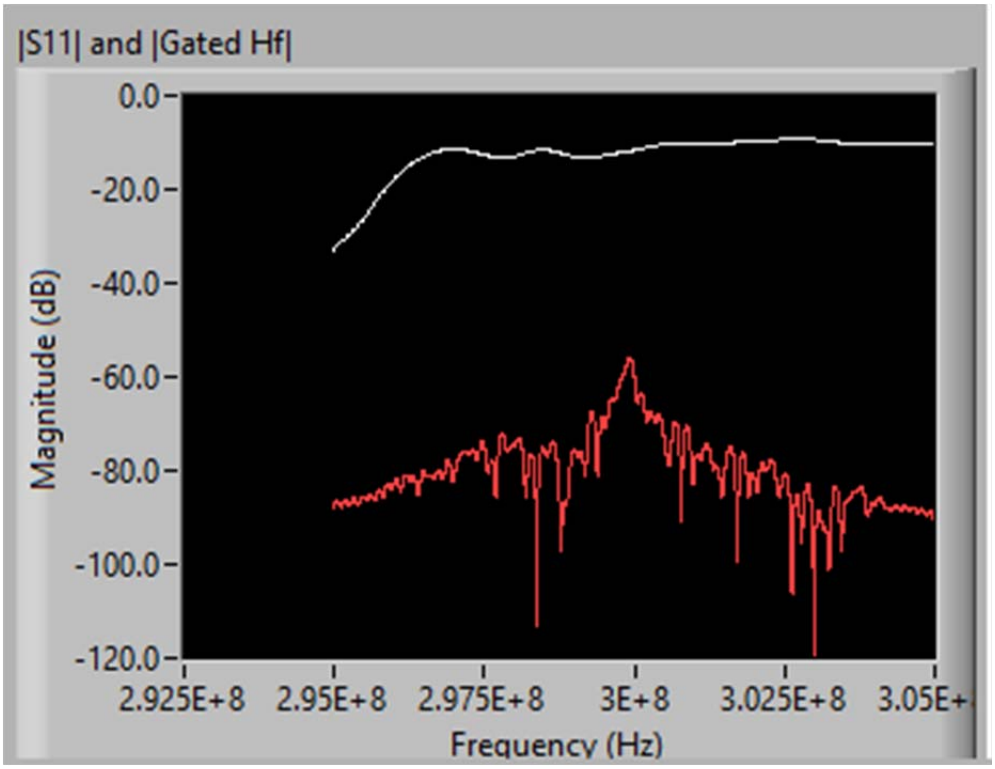

Figure 52: Measured sensor signal mounted at PERC

Table 4: Wireless temperature measurements from two of the installed sensors at the boiler. The PERC thermocouple temperature (TC temp), which is close to the wall of the economizer, and thus far away from the boiler tubes (see Figure 46), is also included in the table for reference.

Date	Device ID	*f* @ RT (MHz)	*f* @ HT (MHz)	Δ*f* (MHz)	Temp (°C)	TC temp (°C)
4/29/16	PERC-3	310.8	307.5	3.3	513	380
5/13/16	PERC-2	322.6	319.8	2.8	465	375

Unfortunately, the data acquisition from the system was interrupted due to an unexpected TriNitroToluene (TNT) blast cleaning which damaged the sensor array packaging structures, as shown in Figure 53. Figure 53 left shows one of the sensor array structures attached to a boiler tube, heavily coated with ash, and missing its ceramic cover after TNT explosive cleaning of the boiler tubes was performed close to the sensor package. Figure 53 Top-right shows one of the ceramic casings from one of the sensor array elements after the TNT blasting. Figure 53 bottom-right is one of the sensor array element and antenna fixture: parts of the ceramic cover have remained attached at the screw locations, revealing where the ceramic casing broke due to the explosive cleaning process. Figure 54 shows one sensor package mounted on the boiler tubes that retained the ceramic cover after the TNT blasting. But unfortunately, even this case was cracked, which compromised the sensor inside.

Figure 53: (Left) One of the sensor array structures attached to a boiler tube, heavily coated with ash, and missing its ceramic cover after TNT explosive cleaning of the boiler tubes was performed close to the sensor package. Top-right is one of the ceramic casings from one of the sensor array elements after the TNT blasting. Bottom-right is one of the sensor array element and antenna fixture: parts of the ceramic cover have remained attached at the screw locations, revealing where the ceramic casing broke due to the explosive cleaning process.

Figure 54: One sensor package retained a ceramic cover, but it was cracked, which compromised the sensor inside.

Yet another mounting structure was devised and is shown in Figure 55. Since another power plant shut-down was still 10 months away, and therefore only limited access to the Economizer chamber was possible, Environetix/UMaine devised another mounting fixture for a sensor package, shown in Figure 55. The interrogating antenna was modified and only one new sensor array was mounted on a tube transversal to the boiling tubes. The temperature to me measured in this case was expected to be close to the temperature measured at the wall of the economizer, since now the sensor is mounted in the middle of the economizer chamber.

Figure 56 shows the temperature measured by the wireless interrogated SAW sensor compared to economizer inlet thermocouple readings for over 40 days, and Figure 57 plots the absolute and percentage differences between the daily temperatures measured by the SAW sensor system and the economizer inlet thermocouple. The average difference between the two datasets is only 1.7%. Given the uncertainties in how close the true temperatures should be at the SAW sensor and thermocouple locations, this is a very small discrepancy and a solid indication that the wireless SAW sensor temperature measurement system is performing extremely well and reliably.

Figure 55: Modified interrogating antenna and a new sensor package installed in the economizer.

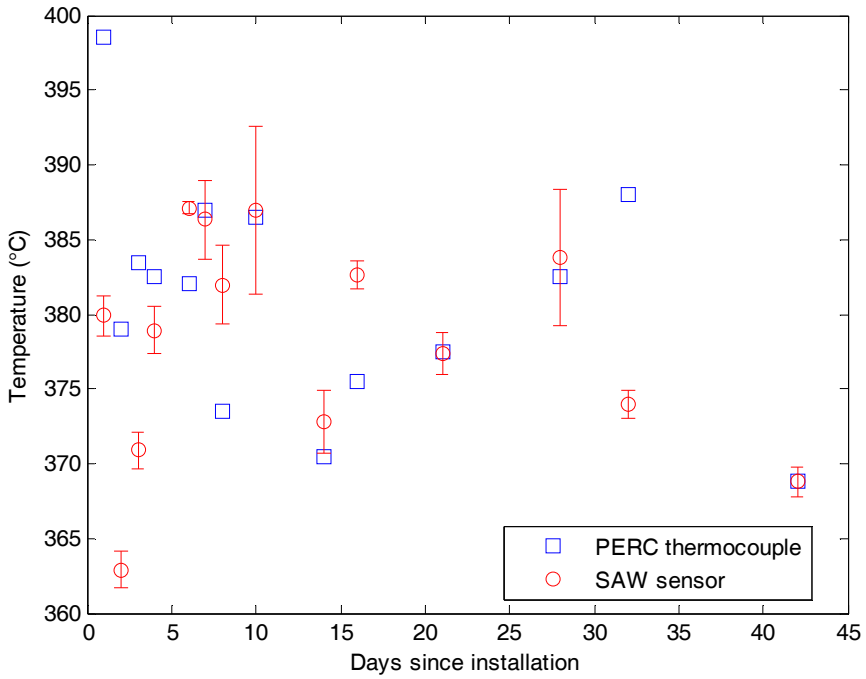

Figure 56: Measured temperature by the wireless interrogated SAW sensor compared to economizer inlet thermocouple readings for over 40 days.

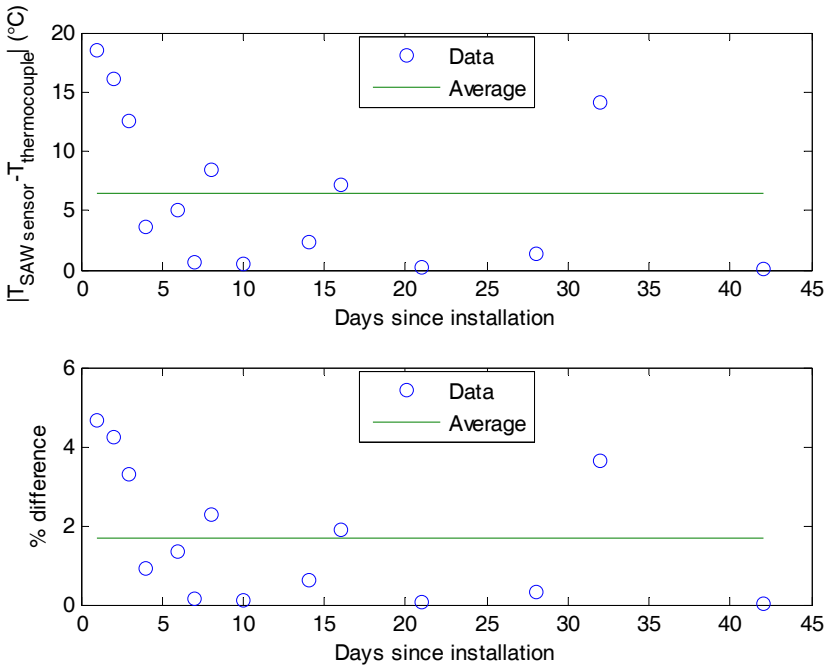

Figure 57: Absolute and percentage differences between the daily temperatures measured by the SAW sensor system and the economizer inlet thermocouple. The average difference between the two datasets is only 1.7%.

6.3 CONCLUSIONS

As reported in this document, the project successfully achieved the targeted goals and objectives of developing and demonstrating the performance of wireless microwave acoustic temperature sensors and arrays, both in laboratory and embedded in meaningful power plant environment, more specifically installed in equipment and structures.

The technology transition to meaningful power plant environments was achieved through two rounds of tests at the NETL Aerothermal facility, Morgantown, WV, and tests throughout two years and a half at the Penobscot Energy Recovery Company (PERC) power plant, Orrington, ME, which is a municipal solid waste (MSW) power plant. The project was performed jointly by the University of Maine and Environetix Technologies Corporation.

The small, battery-free surface acoustic wave (SAW) sensors, integrated antennas, and arrays, comprised of novel materials that are stable in high-temperature harsh environments, have been successfully embedded directly into power generation structures and components, and interrogated wirelessly with stand-alone radio frequency (RF) electronics unit located outside the high-temperature harsh environment.

The work was built on patented UMaine wireless microwave acoustic sensor technology that has been demonstrated by the UMaine / Environetix team to operate at 800ºC for 5½ months in laboratory furnaces and up to 700ºC on rotating parts in scaled turbine engines. In order to advance the pre-existing technology, the following efforts have been successfully developed under this project:

A. Advancement of novel thin film nanocomposite electrodes for wireless SAW sensors to achieve stable and reliable operation above 1000ºC.
B. Development of sensor interrogation methods and sensor encapsulation materials and techniques for embedding sensor arrays into power plant components.
C. Demonstration of the viability of prototype sensor arrays and interrogation systems through laboratory furnace and power plant field testing.

At the beginning of the project, the limitation of the pre-existing Pt/Rh/ZrO_2 electrode film stability to temperatures below 1000°C was established, thus justifying the need to research and develop electrode film for higher operational temperature. Out of this effort, several new electrode combinations were investigated and their performance established, as reported in this document. Multi-layered alloy electrodes and a wide range of Pt alloy electrode materials have been screened including Pt or PtRh combined with alloying elements, such as Co, Ni, Cr, Rh, Ta, Ti, Nb, Al, Sn or oxides HfO_2, ZrO_2, Nb_2O_3, Y_2O_3, RuO_2, CeO_2, NiO, CoO, MnO_2. Short-term (4 hours) electrode performance up to 1200°C has been achieved in blanket metallized test samples.

Electrode stability at temperatures approaching 1200°C is challenged by the strong thermodynamic driving forces that cause film agglomeration and interdiffusion phenomena in this temperature regime. In particular, for the Pt-based alloy films studied, it was verified that Pt volatizing in air environment approaching 1200°C is significant, even considering the successful alloy elements that deter the agglomeration. Once the Pt agglomeration takes place, then the Pt volatizing in air is accelerated. This phenomenon could also be observed for the Pt thick paste

used for the contacts.

The maximum operating temperature of the micrometer scale SAW device interdigitated structures was found to be typically 50-100°C lower than the maximum temperature achieved with the uniform blanket deposited electrode films. Selected thin film electrode materials, including PtRh/HfO_2, Pt/Al_2O_3, and PtNi|PtZr have been used to fabricate SAW devices which have successfully operated above 1000°C, up to about 1100°C.

Tests at the Laboratory for Surface Science and Technology at UMaine, and at Environetix laboratories, together with tests in relevant power plant environment at the NETL Aerothermal facility and at the PERC power plant, allowed the research and development of new packaging materials and designs to withstand the targeted power plant harsh-environments.

Wireless sensor and array operation was successfully developed and adapted to operate in different power plant conditions, namely proximity range interrogation (few centimeters), mid-range distance (fraction of a meter), and longer range (few meters) under harsh environment conditions.

The work performed under this project by UMaine in partnership with Environetix regarding harsh-environment wireless SAW sensors and arrays and their successful transition to meaningful power plant environments, confirmed the maturity of the technology researched and developed for power plant applications. The technology achieved a readiness level that grants application in further power plant environments and the development of new types of microwave acoustic based wired and wireless sensors and arrays.

7.) GRAPHICAL MATERIAL LIST

FIGURES

TABLES

8.) REFERENCES **(supporting publications, conference papers, presentations)**

1. A. Maskay, M. Pereira da Cunha, "High-temperature static strain langasite SAWR sensor: Temperaturecompensation and numerical calibration for direct strain reading," Sensors and Actuators A 259 (2017), pp. 34-43, 2017.
2. M. Pereira da Cunha, A. Maskay, R.J. Lad, T. Coyle, and G. Harkay, "Langasite 2.45 GHz ISM Band SAW Resonator for Harsh Environment Wireless Applications," *2016 IEEE Ultrasonics Symposium,* Tours, France, Sept. 18-21, 2016.
3. A. Maskay, M. Pereira da Cunha, "High Temperature Static Strain Microwave Acoustic Sensor ," *2016 IEEE Ultrasonics Symposium,* Tours, France, Sept. 18-21, 2016. (Paper received the ***BEST STUDENT PAPER AWARD***).
4. R.J. Lad, R.T. Fryer, D.M. Stewart, A. Maskay, M. Pereira da Cunha, "Stable Nanocomposite Thin Films for Harsh Environment Wireless Surface Acoustic Wave Sensors," MS&T'16, Materials Science & Technology 2016 Conference & Exhibition, Salt Lake City, UT, October 24, 2016.
5. M. Pereira da Cunha, "Wireless Battery-free Microwave Acoustic Sensors for Harsh Environment Power Plant Applications," 59th ISA POWID/EPRI Symposium, 27-30 June 2016, Charlotte, NC.
6. M. Pereira da Cunha, "*2016 Update: High-Temperature Wireless Sensor Array for Harsh-Environment Power Plant Condition Monitoring Applications*," 2016 Crosscutting Research & Rare Earth Elements, Sheraton Station Square Hotel, Pittsburgh, PA, April 18-22, 2016.
7. R.J. Lad (Invited Talk) "Platinum-Ceramic Nanocomposite Films for Use in High Temperature Harsh Environments," Materials Research Society Fall 2015 Meeting, Symposium R, December 1, 2015.
8. D.J. Frankel, S.C. Moulzolf, M. Pereira da Cunha, R.J. Lad, "Influence of Composition and Multilayer Architecture on Electrical Conductivity of High Temperature Pt-Alloy Films," Surface & Coatings Technology 284 (2015) 215-221.
9. M. Pereira da Cunha, "*High-Temperature Wireless Sensor Array for Harsh-Environment Power Plant Condition Monitoring Applications*," 2015 Cross Cutting Research Review Meeting, DOE / NETL Program / Support of Advanced Coal Research at United States Colleges and Universities, NETL, Morgantown, WV, October 28, 2015.
10. M. Pereira da Cunha, A. Maskay, R.J. Lad, D.J. Frankel, S. Moulzolf, M. Call, and G. Bernhardt "Pt-Ni / Pt-Zr Electrodes for Stable SAW Resonator Operation During Repeated Temperature Cycling up to 1000ºC," *2015 IEEE Ultrasonics Symposium,* Taipei, Taiwan, Oct. 21-24, 2015, DOI: 10.1109/ULTSYM.2015.0028.
11. M. Pereira da Cunha, "High Temperature Passive Wireless Sensor Technology for Harsh Environment Applications," *2015 Future of Instrumentation & Internet*, Arlington, VA, May 04-06, 2015.
12. M. Pereira da Cunha, "Harsh Environment SAW Wireless Sensor Array for Power Plant Applications," *2015 Cross Cutting Research Review Meeting*, Pittsburgh, PA, April 27-30, 2015.

13. D.J. Frankel, S.C. Moulzolf, M. Pereira da Cunha, R.J. Lad, "Platinum-Based Nanocomposite Electrode Thin Films For High Temperature Operation," *International Conference on Metallurgical Coatings and Thin Films*, April 24, 2015.

14. M. Pereira da Cunha and Anin Maskay, "Wireless Battery-free Harsh Environment Sensor System for Energy Sector Applications," 2014 Cross Cutting Research Review Meeting, in http://www.netl.doe.gov/File%20Library/Events/2014/crosscutting/Crosscutting_20140521_1500A_Maine.pdf, May 19-23, 2014.

15. Mauricio Pereira da Cunha, "Nanoelectrodes for High-Temperature Harsh-Environment Wireless Battery-free Sensors," 2014 Material Research Society Fall Meeting, Session GG: Nanomaterials for Harsh Environment Sensors and Related Electronic and Structural Components Design, Synthesis, Characterization and Utilization Boston, MA, Dec. 2014 (*INVITED PAPER*).

16. M. Pereira da Cunha, R. J. Lad, T. B. Pollard, D. McCann, E. McCarthy, P. Prata, R. Kelley, "Wireless Harsh Environment SAW Array System for Power Plant Application," 2014 IEEE International Ultrasonics Symposium, in Proceeding of the Ultrasonics Symp.- IUS, Chicago, pp. 381-384.

17. Scott C. Moulzolf, David J. Frankel, Mauricio Pereira da Cunha & Robert J. Lad, "High temperature stability of electrically conductive Pt–Rh/ZrO_2 and Pt–Rh/HfO_2 nanocomposite thin film electrodes," Microsystem Technologies, ISSN 0946-7076, DOI 10.1007/s00542-013-1974-x, November 12, 2013, Vol. 20, No. 4-5, April 2014, pp. 523-531.

18. Mauricio Pereira da Cunha, "Wireless Sensing in Hostile Environments," *2013 IEEE Joint UFFC, EFTF, and PFM Symposium*, in *Proceeding of the Ultrasonics Symp.- IUS*, Prague, Czech Republic, pp. 1337-1346. (*INVITED PAPER*).

19. P. Davulis, M. Pereira da Cunha, "Langatate Temperature-Compensated BAW Orientations Identified Using High-Temperature Constants," *2013 IEEE Joint UFFC, EFTF, and PFM Symposium*, in *Proceeding of the Frequency Control Symp.- IFCS/EFTS*, Prague, Czech Republic, pp. 996-999.

20. R. Behanan, S. Moulzolf, M. Call, G. Bernhardt, D. Frankel, R. Lad, M. Pereira da Cunha, "Thin Films and Techniques for SAW Sensor Operation Above 1000°C," *2013 IEEE Joint UFFC, EFTF, and PFM Symposium*, in *Proceeding of the Ultrasonics Symp.- IUS*, Prague, Czech Republic, pp. 1013-1016.

21. S. C. Moulzolf, R. Behanan, R. J. Lad, and M. Pereira da Cunha, "Capacitively Coupled IDT for High Temperature SAW Devices," *2013 IEEE Joint UFFC, EFTF, and PFM Symposium,* in *Proceeding of the Ultrasonics Symp.- IUS*, *Prague, Czech Republic*, pp. 255-258.

22. M. Pereira da Cunha, R.J. Lad, T.B. Pollard, D.F. McCann, E.L. McCarthy, D.J. Frankel, S.C. Moulzolf, R. Behanan, G. Bernhardt, M. Call, "Wireless Sensors and Interrogation System for Harsh Environment Static & Dynamic Monitoring of Turbine Engines and Industrial Machinery," *59th International Instrumentation Symposium*, May 13-17, Invited Presentation to the Propulsion Instrumentation Working Group (PIWG), May 16th, 2013.

23. Scott C. Moulzolf , David J. Frankel, Mauricio Pereira da Cunha, Robert J. Lad, "Electrically conductive Pt-Rh/ZrO_2 and Pt-Rh/HfO_2 nanocomposite electrodes for high-temperature harsh environment sensors", *Proceedings SPIE* vol. 8763, 2013.

24. S.C. Moulzolf, D.J. Frankel, G. Bernhardt, M. Pereira da Cunha, and R.J. Lad, "Investigation of high-temperature properties of Pt-Rh-Zr based nanocomposite thin films," *Thin Solid Films*.

25. P. Davulis and M. Pereira da Cunha, "A Full Set of Langatate High-Temperature Acoustic Wave Constants: Elastic, Piezoelectric, Dielectric Constants up to 900°C," *IEEE Transactions on Ultrasonics, Ferroelectrics and Frequency Control*, Vol. 60, No. 04, April 2013, pp. 824-833.

26. P. Davulis and M. Pereira da Cunha, "Temperature-compensated BAW orientations over 500°C on LGT for frequency control and sensor applications," *Electronic Letters*, vol. 49, no. 3, pp. 170-171, Jan. 2013.

27. M. Pereira da Cunha, "*Wireless Microwave Acoustic Sensor System For Condition Monitoring in Power Plant Environments*," DOE / NETL Program: Advanced Fossil Energy Research: Novel Developments In Sensors And Controls For Fossil Energy Power Generation And Fuel Production Technologies, March 12-14, 2012.

28. M. Pereira da Cunha, "*Technology and Product Update: Wireless Sensors for Extreme Environments*," WEB Conference with ExxonMobil, Feb. 02, 2012.

29. M. Pereira da Cunha, "*High-temperature wireless sensor design solutions*," Invited to sit on the panel and motive discussion on the Wed. session of the Wireless workshop at the International Instrumentation Symposium (IIS), La Jolla, CA, June 6, 2012.

30. M. Pereira da Cunha, "*Industrial Insertion of Wireless Microwave Acoustic Sensors and Systems for Harsh Environments*," Strategic Advisory Board (SAB) of the The Propulsion Instrumentation Working Group (PIWG), June 06, 2012.

31. M. Pereira da Cunha, "*Harsh Environment Wireless Microwave Acoustic Sensor Systems for Aerospace, Energy, and Industrial Applications,*" nationwide WebEx presentation for General Electric, June 14, 2012.

32. Scott C. Moulzolf, Roby Behanan, Robert J. Lad, and Mauricio Pereira da Cunha, "Langasite SAW Pressure Sensor for Harsh Environments," *IEEE International Ultrasonics Symposium Proceedings*, 2012, Dresden, Germany, pp.1224-1227.

9.) LIST OF ACRONYMS AND ABBREVIATIONS

- AC: alternated current
- AFM: atomic force microscopy
- Al: aluminun
- ALD: Atomic layer deposition
- Ce: Cerium
- Co: Cobalt
- Cr: chromium
- DOE: Department of Energy
- EBSD: electron backscatter diffraction detector
- FIB: focused ion beam
- Hf: Hafnium
- IDTs: interdigital transducers
- LASST: Laboratory for Surface Science and Technology
- LGS: langasite, La3Ga5SiO14
- MAL: Microwave Acoustic Laboratory
- MHz: Megahertz
- Mn: Manganese
- MSW: municipal solid waste
- Nb: niobium
- NETL: National Energy Technology Laboratory
- Ni: Nickel
- O: Oxygen
- PERC: Penobscot Energy Recovery Company
- Pt: platinum
- QCMs: quartz crystal rate monitors / quartz crystal microbalance
- R&D: research and development
- RF: radio-frequency
- Rh: Rhodium
- SAW: surface acoustic wave
- SED: secondary electrons detector

- SEM: high resolution scanning electron microscopy
- SEM: scanning electron microscopy
- SiAlON: silon
- TC: thermocouple
- Ti: titanium
- TNT: TriNitroToluene
- UMaine: University of Maine
- wt%: percentage in weight
- XRD: X-ray diffraction
- Y: yitrium
- YSZ: yttria-stabilized zirconia
- Zr: zirconium

#o#o#o#o#o#o#o#o#o#o#o#o#o#o#o#o#o#o#o#o#o#o#o#o#o#o#o#o#o#o#o#o#o#o#o#o#o#o#o#